NEUTRON POLARIZATION FROM THE $D(d,n)^3He$ AND $^9Be(d,n)^{10}B$ REACTIONS

by

George Charles Spalek

Department of Physics
Duke University

Date: April 17, 1972

Approved:

Richard L. Walter

Richard L. Walter, Supervisor

Lawrence E. Thomas

Morris Newsom

Frank DeLucia

A dissertation submitted in partial fulfillment of the requirements for the degree of Doctor of Philosophy in the Department of Physics in the Graduate School of Arts and Sciences of Duke University

1972

ABSTRACT

(Physics)

NEUTRON POLARIZATION FROM THE $D(d,n)^3He$ AND $^9Be(d,n)^{10}B$ REACTIONS

by

George Charles Spalek

Department of Physics
Duke University

Date: _____

Approved:

_____

Richard L. Walter, Supervisor

_____

_____

_____

_____

A dissertation submitted in partial fulfillment of the requirements for the degree of Doctor of Philosophy in the Department of Physics in the Graduate School of Arts and Sciences of Duke University

1972

ABSTRACT

NEUTRON POLARIZATION FROM THE $D(d,n)^3He$ AND
$^9Be(d,n)^{10}B$ REACTIONS

by

George Charles Spalek

Accurate neutron polarization angular distributions from the $D(d,n)^3He$ reaction were measured at 6, 8, 10, 12 and 14 MeV. The results show large polarizations near 45^o c.m. increasing from a value of .13 at 6 MeV to .44 at 14 MeV. A shift of the peak polarization from 45^o c.m. towards 40^o c.m. as the energy increases is also seen. Comparison of the obtained polarization distributions with those from the D(d,p)T reaction shows that the neutron polarizations are consistently smaller up to 12 MeV. The implications of this with respect to the concept of charge symmetry of nuclear forces are discussed. In addition the usefulness of the $D(d,n)^3He$ reaction as a source of polarized 8 to 15 MeV neutrons is also discussed.

Polarization angular distributions were measured for the five most energetic neutron groups from the $^9Be(d,n)^{10}B$ reaction at 3 and 3.5 MeV bombarding energies. All these transitions involve the transfer of an $\ell_p=1$

proton. A decrease in structure of the polarization distributions with increasing excitation of the residual nucleus was observed at both energies. At angles less than 50^{o} c.m. the n_o group polarization becomes more negative with increasing energy and there is evidence that the $j_p = \frac{1}{2}$ transfer component of the n_1 group polarization is positive.

Cross sections for ^{9}Be(d,d) elastic scattering were obtained and optical model parameters extracted. Agreement between DWBA calculations using these parameters and ^{9}Be(d,n) polarization and cross section data was minimal. In particular, the j dependence of the neutron polarization was not reproduced. Reasons for the above are discussed.

ACKNOWLEDGMENTS

I wish to express my gratitude to Professor R. L. Walter for his continued interest, support, hospitality, and patience during the course of these investigations. Dr. Thomas Stammbach's help in the data acquisition and discussion of experimental matters is greatly appreciated.

I would especially like to thank Dr. R. A. Hardekopf for the many hours he generously spent in obtaining the ^{9}Be(d,d) elastic scattering data, performing optical model analyses, and in general giving invaluable aid. Dr. John Taylor's help with the data taking, computer, and ^{9}Be target making is gratefully acknowledged.

A debt of gratitude is owed Professor N. R. Roberson for the design of the computer interface and Mr. S. E. Edwards for his excellent maintenance of the computer and associated electronics. Mr. R. Rummel and Mr. M. Smith's maintenance of the accelerators is also appreciated.

Finally, I would like to especially thank my wife Karen for her infinite patience and encouragement during the writing of this work.

This work was supported in part by the U. S. Atomic Energy Commission.

TABLE OF CONTENTS

LIST OF FIGURES

LIST OF TABLES

NEUTRON POLARIZATION FROM THE $D(d,n)^3He$ AND $^9Be(d,n)^{10}B$ REACTIONS

Chapter I

INTRODUCTION

The purpose behind an experimental study in nuclear physics is to provide information about a nuclear system which would shed some light on the understanding of nuclear interactions. Reactions involving nucleon transfer to a few-nucleon target as well as a many-nucleon target can provide information about the nucleon-nucleus interaction although some aspects differ. The reactions $D(d,n)^3He$ and $^9Be(d,n)^{10}B$ were chosen for this particular experimental study because each of them could provide unique information about problems which have created considerable interest lately.

$D(d,n)^3He$.--The very existence of analog states seems to bear out the assumption of the charge independence (and the weaker assumption of charge symmetry) of nuclear forces. The concept of isotopic spin has been a powerful theoretical tool for studying the nucleus and has been based on this assumption. However there is some evidence, even though inconclusive as yet, that this assumption is not valid. In elastic scattering it is found (Perey, 1970) that the effective interactions for the proton and the neutron differ even after corrections for the Coulomb force are made. As Barschall (1966) pointed out, there are several other cases, including differences in $^3He(p,p)$ and $T(n,n)$ cross sections, where results appear to contradict the charge independence or symmetry assumption. Wigner (1970) in a conference

summary talk, gave a terse discussion of some of the current difficulties in interpreting data for the above reactions and drawing valid conclusions from them.

A study of the polarization from the D(d,n) reaction was undertaken to provide very accurate data in order to determine if suspected differences (Dubbeldam and Walter, 1961; Niewodniczanski et al., 1963; Porter and Haeberli, 1967) between the neutron polarization and that of the D(d,p)T were real. If the mentioned differences are indeed as large as indicated at 12 MeV, this feature would have some impact on theoretical studies in this mass range. Measurements were made as a function of angle for five deuteron energies from 6 to 14 MeV. As a byproduct, the reaction was evaluated as to its suitability as a monoenergetic polarized neutron source as it is supposed to be the most practical source to provide polarized neutrons from 8 to 15 MeV for deuteron energies from 6 to 14 MeV.

^{9}Be(d,n)^{10}B.--Studies of (d,n) and (d,p) reactions on medium A nuclei have produced a wealth of information which for the most part has been adequately fitted using the Distorted Wave Born Approximation method of calculation. However, this approach has yielded poor results when applied to (d,n) and (d,p) reactions on light nuclei. Some of the difficulties in the reactions involving 1p shell nuclei as targets can be traced to interference from resonances; but even where this effect is expected to be small, DWBA has had some difficulties. Better determination of optical parameters to characterize the interaction was needed as well as new types of information. Earlier experiments at our laboratory concerned the (d,n) reactions on ^{10}B, ^{11}B, ^{12}C, ^{13}C, ^{14}N, ^{15}N, ^{6}Li, and ^{7}Li which were studied by Meier (1969) and Thomason (1969). Of the remaining nuclei in the 1p shell only ^{14}C and ^{9}Be are stable. Measurement of ^{14}C(d,n) would be interesting because

the transfer is nearly a pure j transfer which would check some of the observations of Meier et al. (1970). However the cost of a thick enough ^{14}C target is prohibitive. ^{9}Be is suitable but has been avoided because of the high energy resolution problems involved in its study.

The $^{9}Be(d,n)^{10}B$ reaction offers the unique opportunity to gather information on five $l_p=1$ transfer reactions simultaneously. That is, the transitions to the five lowest states in ^{10}B involve the transfer of a proton with orbital angular momentum $l_p=1$ and a total angular momentum transfer of $j_p=1/2$ and $j_p=3/2$. As shown by Cohen and Kurath (1967), the spectroscopic factors $S_{1/2}$ and $S_{3/2}$ (Figure 1) for the neutron group which leaves ^{10}B in the ground state, hereafter called the "n_o (neutron) group", and the n_2 group correspond to a pure $j_p=3/2$ transfer while the n_4 group involves mainly a $j_p=1/2$ transfer and the n_3 group a $j_p=3/2$ transfer. Unfortunately the n_1 group involves an admixture of large portions of $j_p=1/2$ and 3/2 transfers. The present paper reports on an experimental study of the polarization of these five neutron groups at 3.0 and 3.5 MeV bombarding energy. The results yielded systematic information about the Q dependence, the energy dependence, and some curious j dependences of the polarization. $^{9}Be(d,d)$ elastic scattering data obtained by Hardekopf and the author were fitted to obtain optical model parameters. DWBA calculations for the $^{9}Be(d,n)^{10}B$ reaction were performed using these parameters and compared to cross section and polarization data.

The principles of the polarization measurements and the experimental details are handled in chapters II and III for both reactions. Comparison of the D(d,n) data with D(d,p) data and the extraction of the polarization are handled in chapter IV. The remaining chapters are reserved for a discussion of the $^{9}Be(d,n)$ reaction and results.

Figure 1. Energy Levels of ^{10}B

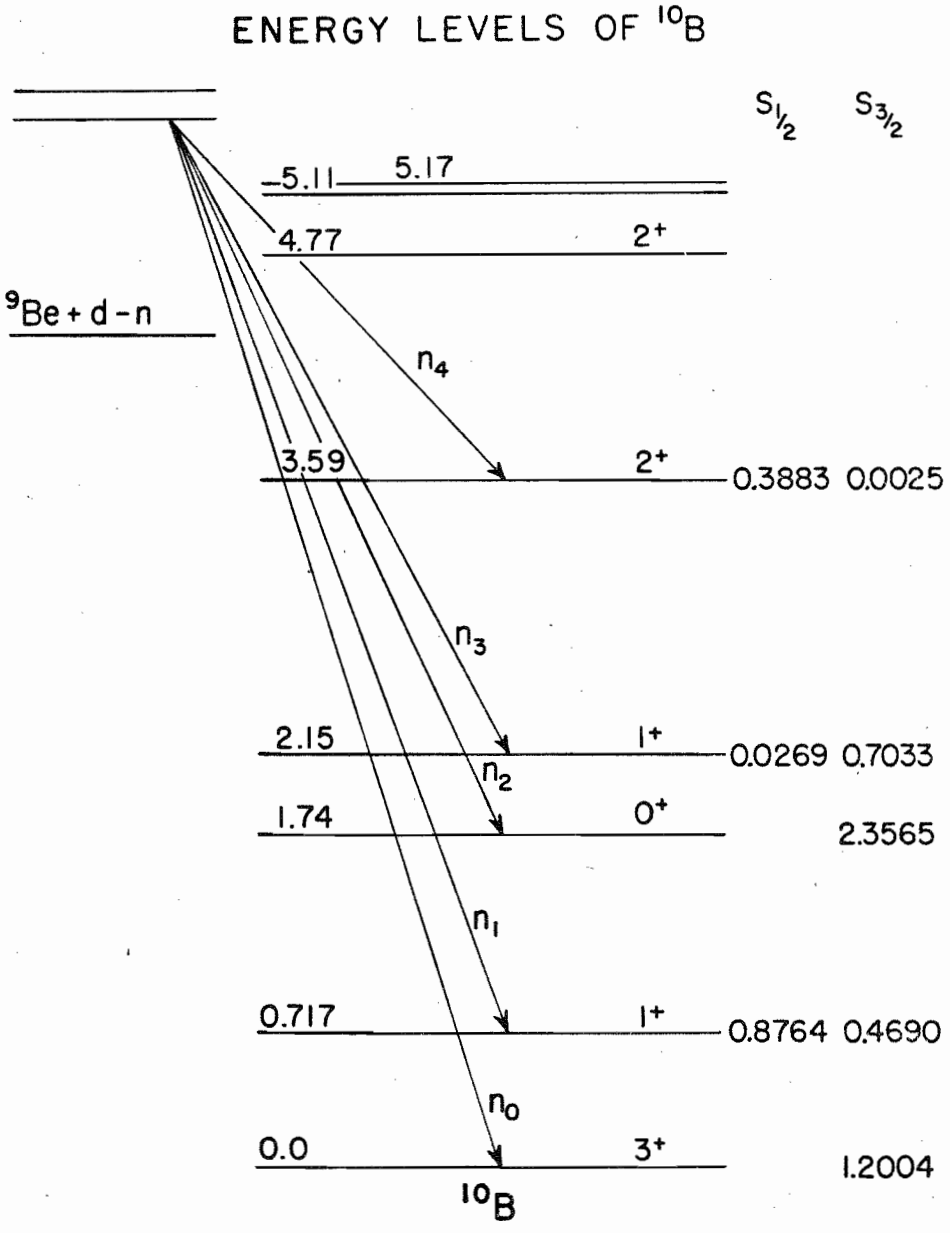
ENERGY LEVELS OF ^{10}B
$S_{1/2}$
$S_{3/2}$
5.11
5.17
4.77
2+
$^{9}Be + d - n$
n_4
3.59
2+
0.3883 0.0025
n_3
2.15
1+
0.0269 0.7033
n_2
1.74
0+
2.3565
n_1
0.717
1+
0.8764 0.4690
n_0
0.0
3+
1.2004
^{10}B

Chapter II

PRINCIPLES OF THE POLARIZATION MEASUREMENT

A. Description of Polarization

In the experiments described in this paper, a beam of deuterons, of momentum $\vec{k}_{1i}$, whose spins are randomly oriented initiates a neutron producing reaction. Neutrons, of momentum $\vec{k}_{1f}$, are detected at an angle θ_1 relative to the incident beam direction as shown in Figure 2. The only physically determined axial vector for an unpolarized incident beam is the one perpendicular to the reaction plane containing the vectors $\vec{k}_{1i}$ and $\vec{k}_{1f}$. The unit vector perpendicular to the reaction plane is defined by:

$$\hat{n}_1 = \frac{\vec{k}_{1i} \times \vec{k}_{1f}}{|\vec{k}_{1i} \times \vec{k}_{1f}|}$$

If the neutron beam emitted from the reaction has a number N_+ of neutrons with spin projection +1/2 along $\hat{n}_1$ (spin parallel to $\hat{n}_1$) and a number N_- of neutrons with spin projection -1/2 along $\hat{n}_1$ (spin anti-parallel to $\hat{n}_1$) the polarization of the beam is defined (according to the Basel (1961) convention) as:

$$P_1(\theta_1) = \left(\frac{N_+ - N_-}{N_+ + N_-}\right) \hat{n}_1 = P_1(\theta_1)\, \hat{n}_1$$

Figure 2. Scheme of Double Scattering Experiment

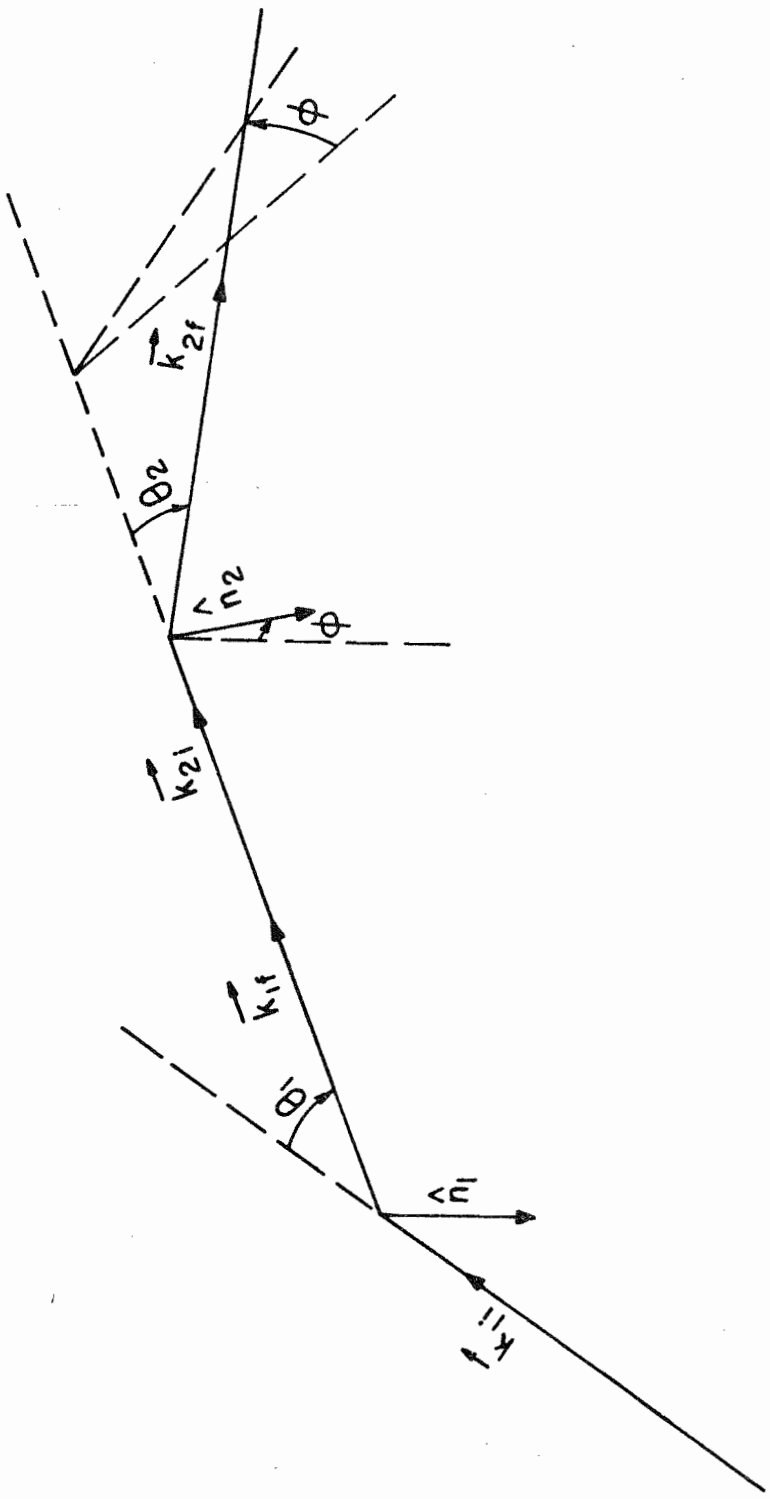
θ
$\vec{k}_{2f}$
θ_2
$\langle \vec{n}^2 \rangle$
θ
$\vec{k}_{2i}$
$\vec{k}_{1f}$
θ_1
$\langle \vec{n}^1 \rangle$
$\vec{k}_{1i}$

B. Polarization Analyzers

Under certain conditions, a scatterer such as ^{4}He elastically scatters neutrons with a given spin orientation preferentially in one direction and those with opposite spin orientation preferentially in the opposite direction. Thus, if the incident neutron beam is polarized, the scattered flux will be greater on one side than the flux scattered through a like angle on the opposite side of the incident beam axis. The magnitude of this asymmetry is related to the beam polarization and the analyzing power of the scatterer.

To illustrate the use of ^{4}He as an analyzer consider Figure 2. The polarized neutron beam from the reaction is scattered off a ^{4}He target. Vectors $\vec{k}_{2i}=\vec{k}_{1f}$ and $\vec{k}_{2f}$ represent the momenta of the incident and (second) scattered beams respectively. The normal to the second plane, i.e. the analyzing plane, is:

$$\hat{n}_2 = \frac{\vec{k}_{2i} \times \vec{k}_{2f}}{\left|\vec{k}_{2i} \times \vec{k}_{2f}\right|}$$

Angles θ_2 and ϕ denote the second scattering angle and azimuthal angle respectively with ϕ defined as:

$$\cos\phi = \hat{n}_1 \cdot \hat{n}_2$$

Assume that the differential cross section for scattering neutrons with spins parallel to $\hat{n}_2$ is σ_+ and the corresponding cross section for neutrons with spins anti-parallel to $\hat{n}_2$ is σ_-. For scattering to the right, $\phi = 0$ and $\hat{n}_1 \parallel \hat{n}_2$. Then N_+ and N_- are the number of neutrons with spins

parallel and anti-parallel to $\hat{n}_2$ respectively. Thus the number of neutrons scattered to the right is:

$$N_R = N_+ \sigma_+ + N_- \sigma_-$$

For scattering to the left, $\hat{n}_1$ is directed opposite to $\hat{n}_2$. Therefore N_+ and N_- are now the number of neutrons with spins anti-parallel and parallel to $\hat{n}_2$ respectively. So the number of neutrons scattered to the left is:

$$N_L = N_+ \sigma_- + N_- \sigma_+$$

The right-left ratio is then:

$$\epsilon = \frac{N_R}{N_L} = \frac{N_+ \sigma_+ + N_- \sigma_-}{N_+ \sigma_- + N_- \sigma_+}$$

which can be put into the form:

$$\epsilon = \frac{1 + \left(\frac{N_+ - N_-}{N_+ + N_-}\right)\left(\frac{\sigma_+ - \sigma_-}{\sigma_+ + \sigma_-}\right)}{1 - \left(\frac{N_+ - N_-}{N_+ + N_-}\right)\left(\frac{\sigma_+ - \sigma_-}{\sigma_+ + \sigma_-}\right)}$$

But $(\sigma_+ - \sigma_-)/(\sigma_+ + \sigma_-)$ is exactly the polarization of an initially unpolarized beam elastically scattered from the ^{4}He analyzer through an angle θ_2.

Defining:

$$\vec{P}_2(\theta_2) = \frac{\sigma_+ - \sigma_-}{\sigma_+ + \sigma_-} \hat{n}_2$$

then the expression becomes:

$$\epsilon = \frac{1 + P_1(\theta_1)\, P_2(\theta_2)}{1 - P_1(\theta_1)\, P_2(\theta_2)}$$

A more useful experimental quantity is the asymmetry ε:

$$\epsilon = \frac{N_R - N_L}{N_R + N_L} = \frac{r - 1}{r + 1}$$

The resulting expression, after some manipulation, is:

$$\epsilon(\theta_1, \theta_2) = P_1(\theta_1)\, P_2(\theta_2)$$

Thus, if P_2, the analyzing power of the second scatterer, can be computed, the polarization of the neutron beam can be determined from the measured asymmetry.

Because all detectors and scatterers are of finite size, the analyzing power P_2 is replaced by an average analyzing power $\overline{P}_2$ obtained by averaging P_2 over the experimental analyzer geometry.

Since the only component of $\vec{P}_1$ that is effective in the second scattering is the one in the direction of $\hat{n}_2$, a replacement of P_1P_2 by $P_1\overline{P}_2(\hat{n}_1 \cdot \hat{n}_2)$ generalizes the above expressions to the case where the second scattering plane forms an angle ϕ with the first scattering plane. Thus:

$$\epsilon(\theta_1, \theta_2) = P_1(\theta_1)\, P_2(\theta_2)\, (\hat{n}_1 \cdot \hat{n}_2)$$

or, for an actual measurement:

$$\overline{\epsilon}(\theta_1, \theta_2) = P_1(\theta_1)\, \overline{P_2(\theta_2)}\, \cos\phi$$

For our purposes, we will replace the measured asymmetry, $\overline{\varepsilon}$, by the customary symbol ε, and make any necessary distinctions later.

C. Spin Precession and Elimination of Instrumental Asymmetries

The experimental determination of the asymmetry in the second scattering process presents two problems: a) neutron detector efficiencies are difficult to accurately determine absolutely; and b) the two detectors monitoring the asymmetry view different direct neutron fluxes from the source reaction because of the change of the neutron production cross section with respect to θ_1. To solve problem b), the detectors could be placed in a plane perpendicular (vertical) to the source reaction plane but then the analyzing power P_2 is zero because $\cos 90^\circ = 0$. Problem a) could be solved by interchanging the two "side" detectors so that there would be no need to know their efficiencies. An elegant method of attaining both objectives without introducing false asymmetries by inaccurate physical interchange of side detectors was proposed and used by Hillman et al. (1956). The analyzing plane is made vertical by placing the side detectors at equal angles above and below the horizontal He-scattering plane. Then the polarization vector of the neutron beam from the reaction is Larmour precessed by $+90^\circ$ about the beam axis using a solenoidal magnetic field and an asymmetry measurement is performed. This measurement is entirely equivalent to the one using a horizontal analyzing plane and unprecessed neutron polarization vector. If the solenoidal magnetic field is reversed the polarization vector is rotated by -90°. The resulting asymmetry measurement is identical to the previous one but the roles of the up and down detectors have been effectively interchanged.

A new up and down ratio can be defined:

$$r = \sqrt{\frac{UF \cdot DR}{DF \cdot UR}} = \sqrt{\frac{I_{UF}\, n_U}{I_{DF}\, n_D} \cdot \frac{I_{UR}\, n_D}{I_{DR}\, n_U}}$$

where UF is the number of neutrons detected in the UP detector, the solenoidal magnetic field being in the "forward" direction. I_{UF} is the number of neutrons scattered into the UP detector (with the magnetic field in the "forward" direction) whose detection efficiency is n_U. If neutrons are detected in the side detectors in coincidence with the corresponding ^{4}He recoils, the efficiency of the coincidence circuitry is included in n_U. Similar definitions obviously follow for the other symbols.

It can be seen from the equation that, unless the detection efficiencies are affected by the polarity of the magnetic field or changes in time of the coincidence requirements, they cancel and need not be determined. Furthermore, under these conditions no false asymmetries are introduced by counting longer with the neutron spins precessed through one angle than through the opposite angle. A very important feature of the solenoid method is that the asymmetry measurement can be automated so that the spin direction can be reversed at frequent intervals and the whole data recording process can be put under computer control, as discussed later.

In practice, the polarized beam is sometimes too energetic for the solenoidal magnetic field to precess the polarization vector by a full 90°. If the angle of precession is ψ then the component of P_1 perpendicular to the analyzing plane is $P_1 \cos(\frac{\pi}{2} - \psi) = P_1 \sin\psi$. Then:

$$\epsilon = P_1 P_2 \sin\psi \quad , \quad P_1 = \frac{\epsilon}{P_2 \sin\psi}$$

The factor $\frac{1}{\sin\psi}$ is called the spin correction factor (SPCF), and can be calculated from the neutron energy and the magnetic field strength.

Chapter III

EXPERIMENTAL APPARATUS AND TECHNIQUES

A. General Description

The experimental arrangement used to study both the $^{9}Be(d,n)^{10}B$ and the $D(d,n)^{3}He$ reaction is shown in Figure 3. Polarized neutrons emerging at a variable reaction angle θ_1 had their spins precessed through about 90^{o} in a longitudinal magnetic field produced by a solenoid. After passing through the solenoid the neutrons were incident on a high pressure helium scintillation cell. Those neutrons scattered through the desired analyzing angle Θ_2 were detected by a pair of scintillation side detectors. Coincidence and pulse height requirements had to be met before a count could be used in computing the asymmetry in the counting rates of the side detectors.

B. Accelerators and Targets

$^{9}Be(d,n)$ Reaction--Deuterons were accelerated by the Triangle Universities Nuclear Laboratory (TUNL) 4 MV Van de Graaff accelerator. After being momentum analyzed through 60^{o} in a magnetic field the beam was collimated by two 0.48 cm diameter collimators placed at 30.5 cm and 61.0 cm from the ^{9}Be target. The accelerator voltage was measured with a precision generating voltmeter which had been calibrated at the $^{7}Li(p,n)$ threshold.

Figure 3. Polarimeter

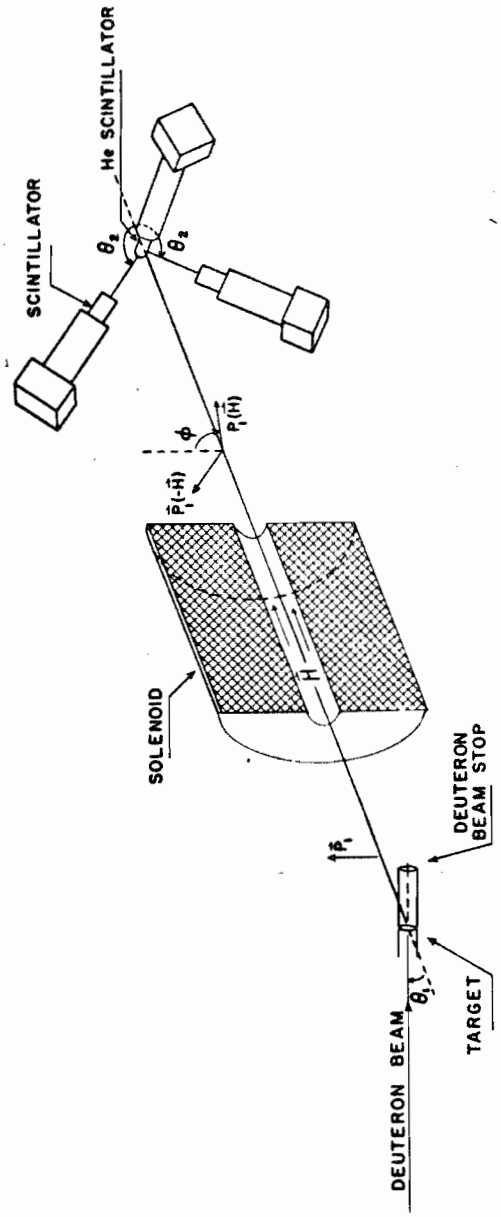
He SCINTILLATOR
SCINTILLATOR
θ_2
θ_2
$\vec{P}_1(\vec{H})$
ϕ
$\vec{P}_1(-\vec{H})$
H
SOLENOID
DEUTERON BEAM STOP
$\vec{P}_1$
θ_1
TARGET
DEUTERON BEAM

The targets consisted of ^{9}Be evaporated onto a 0.025 cm thick tantalum backing and had a thickness corresponding to an energy loss of 60 keV for 3.5 MeV deuterons. Appendix A describes the evaporation and thickness measuring techniques.

A target wobbler was designed and constructed permitting circular movement of the water cooled target so that 4 μa of 4 MeV beam could be used with no target deterioration. Wobble radii could be varied to expose new areas of the target. Target condition was monitored through glass viewing ports in the wobbler. Electrons back-streaming from the target were suppressed by applying -300 v to an insulated section of the wobbler close to the target. This permitted accurate beam current and charge integration measurement.

D(d,n) Reaction--The deuteron beam from the TUNL 7.5 MV tandem electrostatic accelerator was momentum analyzed through 59°. Beam energies were determined by measuring the field in the analyzing magnet with a standard NMR probe. The relative currents from three insulated collimators of sizes 0.64 cm, 0.48 cm, and 0.48 cm respectively placed at distances of about 66 cm, 61 cm and 25.4 cm from the deuterium gas target allowed monitoring of the beam diameter.

Targets consisted of deuterium gas contained in a 4.5 cm long stainless steel cylinder with 6 μm thick Havar[1] beam entrance and exit windows. A tantalum disk stopped the beam 10 cm beyond the gas target. Gas pressures were maintained at 3.7 atm absolute and checked frequently. Diffusion of the deuterium through the beam heated foil windows never changed the pressure by more than 1%. Beam energy losses to the center of the gas targets (including energy loss in the foil window) were 455, 400, 339, 302,

[1]Havar is a high strength cobalt alloy sold by the Hamilton Watch Company, Pittsburgh, Penn.

and 250 keV at beam energies of 6.455, 8.400, 10.339, 12.302, and 14.250 MeV respectively. An air-water spray was used to cool the gas cell and beam stop.

The deuteron beam current was usually 3 to 4 μa. When data were taken at reaction angles less than 25^{o} (lab.), the beam current had to be lowered to 1 μa or less; otherwise the detector electronics would not operate reliably in the high neutron flux present at these angles.

C. Solenoid

The solenoid used to precess the ^{9}Be(d,n) neutron spin, as discussed in chapter II, was similar to one described by Sawers (1966). It consisted of 3 sections with a 5.1 cm diameter center hole surrounded by an Armco iron flux return box 3.18 cm thick on the ends and 0.95 cm thick on the sides and top. The bottom was left open to provide room for cooling water, current, and thermal and overcurrent protection connections. This shielding reduced the fringing fields in the region of the neutron detectors to about one gauss. Power was provided by a 35 KW, 325 ampere motor-generator set whose field coil current, and therefore output, was set by a 0-3 A computer-controlled field coil power supply built by Thomason (1969).

Since the D(d,n) neutrons produced in the tandem lab were more energetic than the ^{9}Be(d,n) ones, a larger magnetic field was needed to precess their spins within a reasonable distance. To this end, a new 75 KW 600 ampere MG set was installed in the TUNL Tandem Accelerator Laboratory (Appendix B) and a fourth coil was added to the solenoid. The field coil supply was retained with only slight alterations. Fringing fields near the neutron detectors for this larger solenoid were measured with a Hall probe and were found to be less than 2 gauss.

In order to determine the current needed to precess the spin of a given energy neutron by 90^{o}, both solenoids were calibrated using polarized neutrons of a low energy. The $^{12}C(d,n)$ reaction was used to produce highly polarized neutrons. Asymmetry measurements were performed for various solenoid current settings ranging from 0 to 300 A. A plot of the measured asymmetry versus solenoid current should obey the equation:

$$\epsilon = \epsilon_{o} \sin\left(\frac{k\, I_{sol}}{\sqrt{E_{n}}}\right)$$

where ε_{o} is the maximum value of the asymmetry, I_{sol} is the solenoid current, E_{n} is the neutron lab. energy and k is a constant for the particular solenoid used. A program was written which adjusted the values of ε_{o} and k for best least squares fit to the data. The same program also computed the current required to precess the spin of neutrons of given energies by 90^{o} for use in setting the solenoid current during the experiments and computing the spin precession correction factor (SPCF). Figure 4 shows the data, fit, and results for the 3 coil configuration.

Approximately 2.5 cm of lead shielding and 10 cm of paraffin were inserted behind the solenoid box to decrease the direct γ-ray and neutron fluxes to the polarimeter side detectors. A tapered polyethylene collimator was also inserted into the center of the solenoid. The taper was adjusted so that a 2.5 cm radius circular section of the He scintillator was illuminated by the neutron beam. Wider neutron beams were not desirable since neutrons scattered from the thicker steel portions of the He scintillator would change the measured asymmetry values and the accidental background rate. Both effects would increase the uncertainty in the final polarization values.

Figure 4. Solenoid Calibration

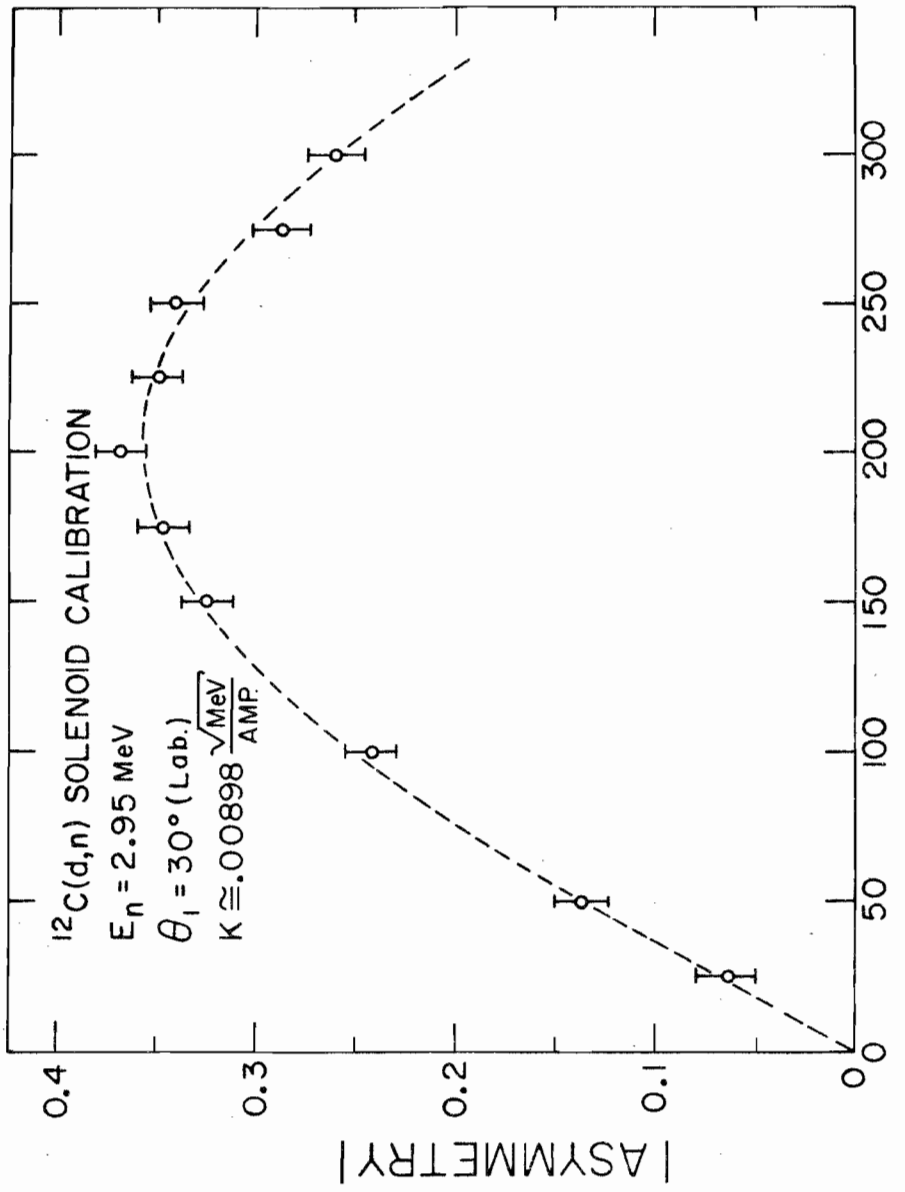
$^{12}C(d,n)$ SOLENOID CALIBRATION
$E_n = 2.95$ MeV
$\theta_1 = 30°$ (Lab.)
$K \cong .00898 \frac{\sqrt{MeV}}{AMP}$
| ASYMMETRY |
0.4
0.3
0.2
0.1
0
0
50
100
150
200
250
300
I_{SOL} (amp.)

D. Polarimeter

A general description of the polarimeter has already been given. The individual parts will now be described.

Helium Cell--The design of the high pressure helium scintillation cell used in the present experiment is similar to the one described by Shamu (1962). The cell was machined from a solid block of type 304 stainless steel and had a 0.22 cm wall thickness in the sensitive volume region. The polished interior of the cell was coated with a 2 mm thick MgO layer which served as a good diffuse reflector. The open end of the cell was closed with a Teflon "O" ring-sealed 1.9 cm thick tempered glass disc and a 0.95 cm thick backup plate of Lucite. Since the He gas scintillations have wavelengths in the ultra-violet region of the spectrum where Lucite light-pipes and ordinary photomultipliers are very inefficient, a layer of wavelength shifter (p-p' diphenyl-stilbene) was evaporated onto the MgO coated cell. The wavelength shifter thicknesses varied from approximately 400 mg/cm^2 on the end opposite the window to 300 mg/cm^2 near the window. A layer of about 25 mg/cm^2 was also evaporated onto the inside of the window.

The cell was pumped down to 10^{-6} torr, heated, and allowed to outgas for two days before filling with a mixture of He and Xenon gas. Both gases were purified by passage through a molecular sieve. The molecular sieve was at liquid nitrogen temperature for the He purification and at dry ice temperature for the Xe purification (the Xe would condense and solidify at liquid nitrogen temperatures). The gas pressures were 93 atm of He and 10 atm of Xe for the ^{9}Be(d,n) experiment and 110 atm He and 6 atm Xe for the D(d,n) experiment.

An RCA 6810-A photomultiplier viewed the He cell through a tapered light-pipe. The photomultiplier (PM) was enclosed in an Armco iron cylinder which eliminated the stray solenoid magnetic fields that could affect the gain of the PM tube. A Lucite sleeve was used to insulate the PM tube with its high voltage electrostatic shield from the Armco cylinder. The stray magnetic fields were measured under experimental conditions inside the Armco cylinder and were found to be less than 0.1 gauss.

Two signals were derived from the outputs of the photomultipliers. One signal ("Linear" or "Slow" signal) was proportional to the ^{4}He recoil energy resulting from a scattering event in the cell. The other was a "Fast" (2 ns risetime) signal useful for timing purposes.

Side Detectors--The side neutron detectors were 15.2 x 7.6 x 5.0 cm^3 NE-213 liquid scintillators and identical size NE-102 plastic scintillators for the ^{9}Be(d,n) and D(d,n) reactions respectively. The magnetic shield, photomultiplier, Lucite insulator, and light-pipe arrangements were similar to the He cell set-up. Again stray magnetic fields inside the Armco cylinders were less than 0.1 gauss at maximum solenoid currents. Only the "Fast" signals were derived from the photomultiplier outputs.

The distance from the center of the side detector to the center of the He cell was 29 cm for the ^{9}Be reaction and 19 cm for the D(d,n) reaction. These particular distances were chosen since they represented a good compromise between the following effects: a) "tight" geometry gives desirable, large coincidence counting rates; b) large side detector to He cell distances improve the energy resolution (due to finite detector sizes) of the polarimeter permitting separation of different energy neutron groups; c) large distances allow better time-separation of neutron and γ-ray events by coincidence circuitry.

The analyzing angle θ_2 was chosen to be 120^o lab. At this neutron scattering angle, the ^{4}He recoils are very energetic and the ^{4}He analyzing power P_2 and cross section $\sigma(\theta_2)$ are such that $[P_2(\theta_2)]^2\sigma(\theta_2)$ has a relative maximum. The high value of $P_2{}^2\sigma$ minimizes the time needed to obtain an asymmetry to a given degree of precision, the time being inversely proportional to $P_2{}^2\sigma$.

E. Electronics

A block diagram of the electronics is shown in Figures 5 and 6. This system was similar for the two reactions studied so only the D(d,n) system will be described.

Fast pulses from the UP detector, for example, were amplified before input into a fast discriminator. The energy level of the discriminator was adjusted by varying the photomultiplier high voltage. Using a ^{137}Cs 661 keV γ-ray source and an oscilloscope, the threshold was set at the Compton edge energy. This corresponds to the maximum recoil energy of a proton after interaction with a 1.6 MeV neutron. For the Be reaction, this bias level was lowered to 0.16 MeV proton energy in view of the lower neutron energies.

The discriminator output pulses were clipped to 5 ns and triggered an updating discriminator which was used as a three-way fan-out to provide three outputs. Two of the outputs, one delayed by 50 ns, were fed into a four-input coincidence unit strobed by a properly delayed signal generated in like manner by the fast Helium pulses. Adjustment of delays will be described later. The coincidence output from the helium and UP detectors pulse (He + UP) corresponds to an event where a neutron scattered from the He analyzer and was detected in the UP detector. The other coincidence signal

Figure 5. Fast Electronics

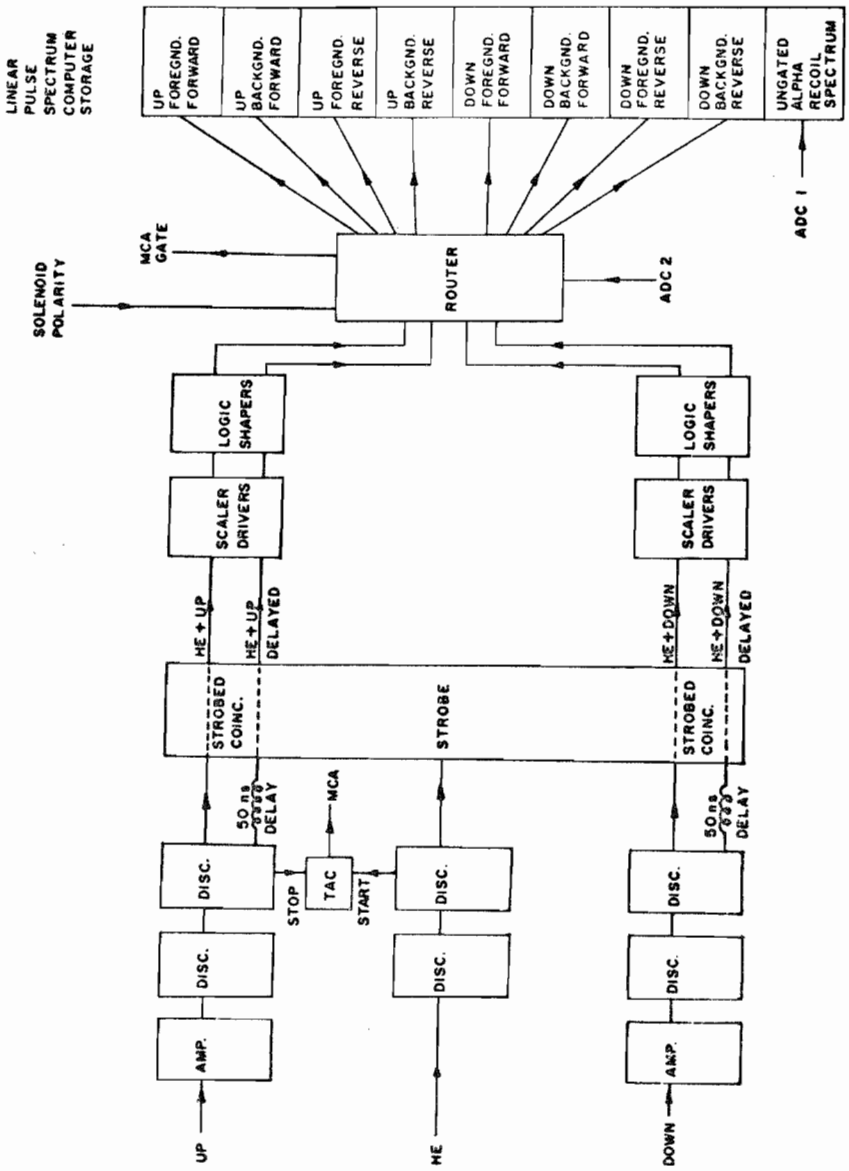
LINEAR PULSE SPECTRUM COMPUTER STORAGE
UP FOREGND. FORWARD
UP BACKGND. FORWARD
UP FOREGND. REVERSE
UP BACKGND. REVERSE
DOWN FOREGND. FORWARD
DOWN BACKGND. FORWARD
DOWN FOREGND. REVERSE
DOWN BACKGND. REVERSE
UNGATED ALPHA RECOIL SPECTRUM
ADC 1
MCA GATE
SOLENOID POLARITY
ROUTER
ADC 2
LOGIC SHAPERS
SCALER DRIVERS
HE + UP
HE + UP DELAYED
HE + DOWN
HE + DOWN DELAYED
STROBED COINC.
STROBE
50 ns DELAY
MCA
STOP
TAC
START
DISC.
AMP.
UP
HE
DOWN

Figure 6. Linear Electronics

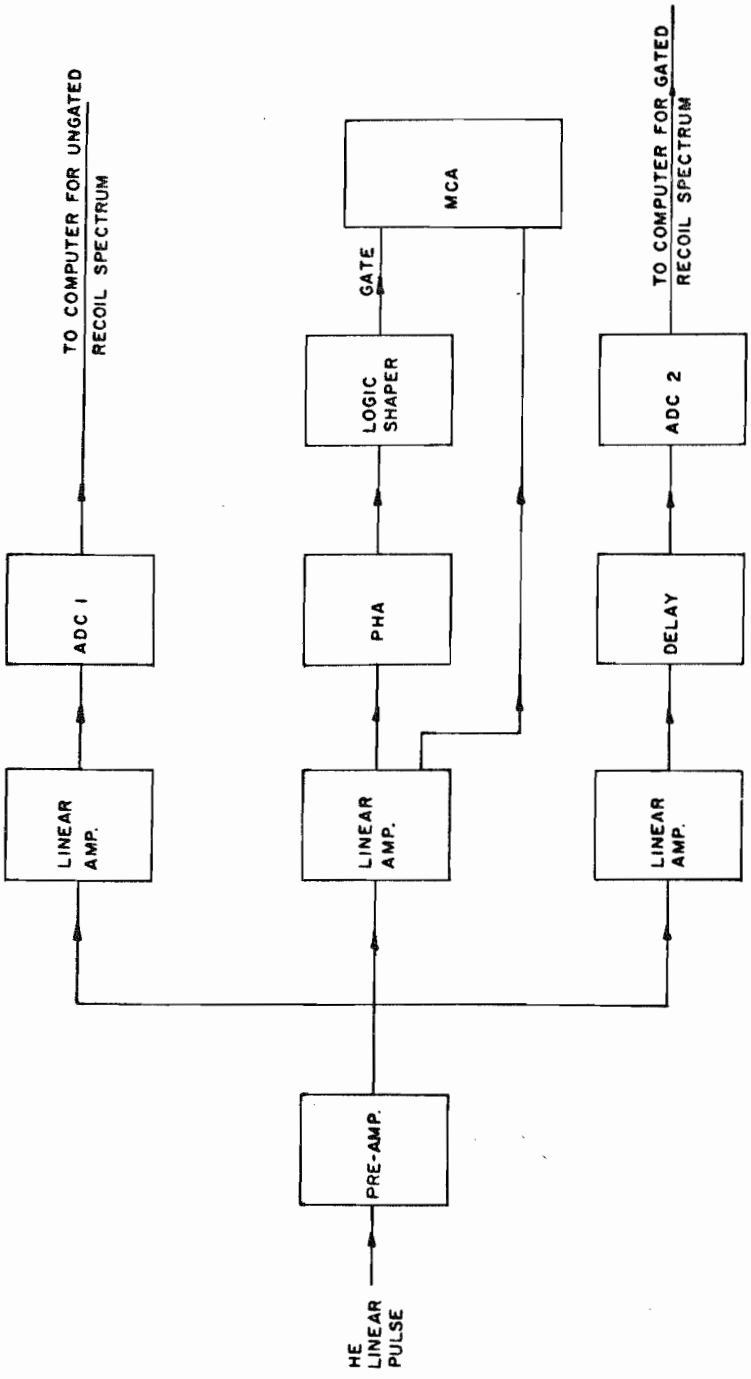
HE LINEAR PULSE
PRE-AMP.
LINEAR AMP.
LINEAR AMP.
LINEAR AMP.
ADC 1
PHA
DELAY
LOGIC SHAPER
ADC 2
MCA
GATE
TO COMPUTER FOR UNGATED RECOIL SPECTRUM
TO COMPUTER FOR GATED RECOIL SPECTRUM

(He + UP delayed) corresponds to an accidental coincidence from random events in the UP and the He scintillators.

The coincidence circuitry for the UP and DOWN detectors was identical except for slight differences in the delay and high voltage settings.

The amplified slow He signal was interfaced (Figure 6) to the TUNL DDP-224 on-line computer through two analog-to-digital converters (ADC). The four fast coincidence outputs gated ACD2 and routed the digitized He signal to separate memory sections (Figure 5). Thus four 128 channel He-recoil coincidence spectra were formed simultaneously for each solenoid field polarity. A sum spectrum was also computed by adding together the four spectra after subtraction of the four accidental spectra. In addition a 128 channel ungated alpha recoil spectrum was accumulated through ADC1. All spectra could be displayed on an oscilloscope.

Analyses of spectra from any previous run could be conducted while new data sets were being accumulated. These early values aided in noticing any problems that developed and in determining the need for more data at a specific angle. The final reported values were obtained in a more careful fitting of the spectra which is described in the analysis sections. Asymmetries were extracted from the coincidence-gated spectra as follows. The accidental coincidence spectra were subtracted from the corresponding foreground spectra. In each spectrum the counts in the coincidence peaks were summed between the same light-pen selected channels yielding the quantities UF, DF, UR, and DR. The asymmetries were then computed using these numbers as described in Chapter II. In addition to the previous tasks, the computer, under control of the program PUNJAB of Taylor (1971), was used for: a) monitoring both the beam current and solenoid field polarity and stopping

the data taking if either was incorrect; b) automatic cycling of the solenoid polarity after selected target charge integration intervals; c) automatic data transfer onto magnetic tape after each data set is completed.

Figures 5 and 6 also show the method used in setting the delays in the UP detector circuitry. Helium and UP detector fast pulses were used as "start" and "stop" signals, respectively, for a time to amplitude converter (TAC). The TAC output was analyzed in one quadrant of a 400 channel multichannel analyzer (MCA). The MCA was gated with large amplitude linear pulses from the Helium cell selected by the single channel pulse height analyzer (PHA). This gate conveniently ensured that mostly neutron events of interest were analyzed and that the large number of Compton electrons which have a range in the He gas much larger than the He cell dimensions and therefore produce small pulses do not interfere in the timing adjustment. A peak in this gated TAC spectrum corresponded to a distribution of neutron flight times from the He cell to the UP detector.

Another spectrum of TAC pulses gated by the foreground coincidences showed the time "window" selected by the coincidence unit. By varying the UP detector delay, this window was adjusted to bracket the neutron peak in the first time-of-flight (TOF) spectrum. The background delay was adjusted so that the window bracketed a region where there was no structure on the TOF spectrum. The same procedure was used for the DOWN detector timing adjustment.

By adjusting the updating discriminator pulse widths, the coincidence window width was set at 6 ns for the D(d,n) reaction. This width was increased to 24 ns for the ^{9}Be(d,n) reaction so as to bracket the flight times of all the neutron groups of interest.

Chapter IV

D(d,n) DATA HANDLING AND RESULTS

A. Data Acquisition

The D(d,n) data taking procedure was as follows. Because the counting rates were high, after the deuteron beam was turned on, the photomultipliers were allowed to stabilize by waiting about 5 minutes. The coincidence timing was checked as in Chapter III. With the solenoid in the "forward" polarity, data were taken till a given amount of target charge, corresponding to about a 20 minute time interval, was accumulated. Following this, the solenoid field was reversed and data were taken for an equal amount of charge. The process was then repeated in inverse order, tending to cancel long term drifts. After a selected number of cycles, the spectra were transferred to magnetic tape and punched out on computer cards for off-line analysis. The UP and DOWN detector coincidence counting rates were monitored with scalers during the data taking. The side detector efficiencies were also watched so that any electronics breakdown could be detected immediately. When the polarimeter was placed at a new reaction angle, the above process was repeated.

The measurements at all angles were checked for false instrumental asymmetries by repeating them at the same reaction angle (θ_1) but on the opposite side of the deuteron beam axis ($-\theta_1$). No effect outside of the statistical uncertainty was noticeable.

In addition to the above precautions, the "background" coincidence counts from γ-rays and from neutrons produced in reactions other than the D(d,n) reaction were measured. This measurement was carried out at nearly all angles and energies except at 6 MeV. At 6 MeV the background levels were considered small enough so that a background extrapolated from the 8 and 10 MeV data would introduce negligible error into the polarization values. The neutrons in question arose from the interactions of the deuteron beam with beam collimators, Havar foils, and the beam stop. Even though the collimators and the beam stop were made of Ta, neutrons could be produced by the beam striking the beam-deposited deuterium in the metal. However, the background contribution from these two sources should be small since the He cell did not "see" them directly. In fact, the full thickness of the solenoid shielded the He cell at the angles of the present experiment. Yet neutrons or γ-rays from the target cell materials could reach the He cell at all angles after passing through a relatively small thickness of the tapered neutron collimator in the solenoid. These neutrons and γ-rays could originate from (d,n) reactions with the Havar alloy components. Such neutrons would have unknown polarizations and would contribute a true background to the coincidence gated spectra. Also, neutrons could be produced by interaction of the beam with deuterium embedded in the Havar foils. Due to the small beam energy loss in these foils such neutrons would have almost exactly the same polarization and energy as those of interest and theoretically there would be no need to differentiate them from the "good" neutrons. The γ-rays of course could not produce an asymmetry in the polarimeter but could have produced a non-polarized background under the neutron peak. Because the D(d,n) neutrons are so energetic, the n-γ flight time difference is too small to be resolved completely by the coincidence circuitry. However, the γ produced pulse heights should be low since the

range of Compton electrons in the He cell is much greater than the cell dimensions.

To measure the above "backgrounds", the gas target was evacuated after the foreground data for each angle were complete. Data were then accumulated again under the same conditions as for the foreground measurement but only for about one-third of the integrated charge.

At 8 MeV measurements were also carried out at 20^{o} and 35^{o} (lab) to measure the neutron flux that is scattered from the walls and floor of the target area and gives true coincidence counts. To this end, the solenoid core was plugged with a solid brass cylinder and data were accumulated with the deuterium target filled. The resulting count rates were less than 4.0×10^{-4} of the foreground rates and were therefore negligible.

B. Analysis of Spectra

The procedures used in extracting asymmetries from the data, correcting for backgrounds, and correcting for the finite size of target and He cell will now be described.

Using the computer code PUNJAB of Taylor (1971), the accidental background spectra were subtracted from the corresponding foreground spectra. The channels to be included in the coincidence peaks for the asymmetry calculations were manually selected. Due to the presence of the backgrounds under the coincidence peaks, only the central portions of the peaks were selected so as to obtain the optimum accuracy. The width of this summing region was chosen to be large enough so that the computed average analyzing power for this region was the same as for the entire peak width. Yet the summing region was small enough that the background constituted only a small portion of the total number of counts. The summing region selection

was performed as follows. An estimate of a linear background was made. When this background was subtracted, a gaussian-shaped peak was left in the spectrum. The integration channels were terminated when the number of counts fell below approximately one-third of the gaussian peak height. The four integrated peak areas (including the remaining backgrounds) represented the total counts UF, DF, UR, and DR as defined in chapter II. These were used to compute the UP-DOWN ratio and asymmetry:

$$r = \sqrt{\frac{UF}{DF}\cdot\frac{DR}{UR}} \qquad \epsilon = \frac{1-r}{1+r}$$

The associated statistical errors were also calculated.

Asymmetries for five-channel blocks were also calculated in the region just below the coincidence peaks on the low energy side. These asymmetry values were consistent with zero at all reaction angles. The no-gas spectra were analyzed in identical manner using the same summing channels as in the foreground spectra. These asymmetries were also seen to be consistent with zero at all angles. The five-channel-block asymmetries provided grounds for assuming both the no-gas and the unaccounted for backgrounds (residual background) to be unpolarized.

Final asymmetry values and their uncertainties were extracted by correcting for the various backgrounds as follows. First the asymmetries obtained from the foreground spectra were corrected for the unpolarized no-gas backgrounds. The resultant asymmetries will be labeled $\varepsilon_{\alpha_1} \pm \varepsilon_{\alpha_1}$. Where the ε_{α_1} stands for "asymmetry corrected for background level α_1".

Also the properly scaled no-gas spectra were subtracted directly from the foreground spectra and estimates were made of the upper and lower limits of the remaining unaccounted for backgrounds, α_2 and α_3 respectively. Linear shapes were assumed for these backgrounds. After computing the mean background levels $\bar{\alpha} = \frac{\alpha_1 + \alpha_2}{2}$ the final asymmetry values were computed by correcting ε_{α_1} for the background level $\bar{\alpha}$. To include the effect of the uncertainty in the background level estimated, asymmetries $\varepsilon_{\alpha_1\alpha_2}$ and $\varepsilon_{\alpha_1\alpha_3}$ were computed. The quantity $\frac{1}{2}|\varepsilon_{\alpha_1\alpha_2} - \varepsilon_{\alpha_1\alpha_3}|$ then represented the uncertainty in the final asymmetry values due only to the background estimate uncertainties. This non-statistical uncertainty was added directly to those computed earlier. Symbolically, the expression for the final corrected asymmetry is:

$$\epsilon \pm \Delta\epsilon = \epsilon_{\alpha_1\bar{\alpha}} \pm \left(\Delta\epsilon_{\alpha_1\bar{\alpha}} + \frac{|\epsilon_{\alpha_1\alpha_2} - \epsilon_{\alpha_1\alpha_3}|}{2} \right)$$

Figure 7 shows some of the mentioned spectra. Shown at the top are two of the UP and DOWN coincidence-gated spectra. The squares show the contribution due to the accidental coincidences between the He cell and the side detectors as well as the background due to the presence of the Havar foils. In Figure 8 is shown the sum of the upper spectra with the backgrounds subtracted. A similar spectrum for another angle is also shown. The dashed lines represent the estimated upper and lower limits of the unaccounted for backgrounds.

The final asymmetry values were converted to polarization values in the usual manner by multiplying by the spin correction factor and dividing by the average analyzing power. The phase shifts of Stammbach and Walter (1971)

Figure 7. D(d,n) UP and Down Coincidence-Gated Spectra

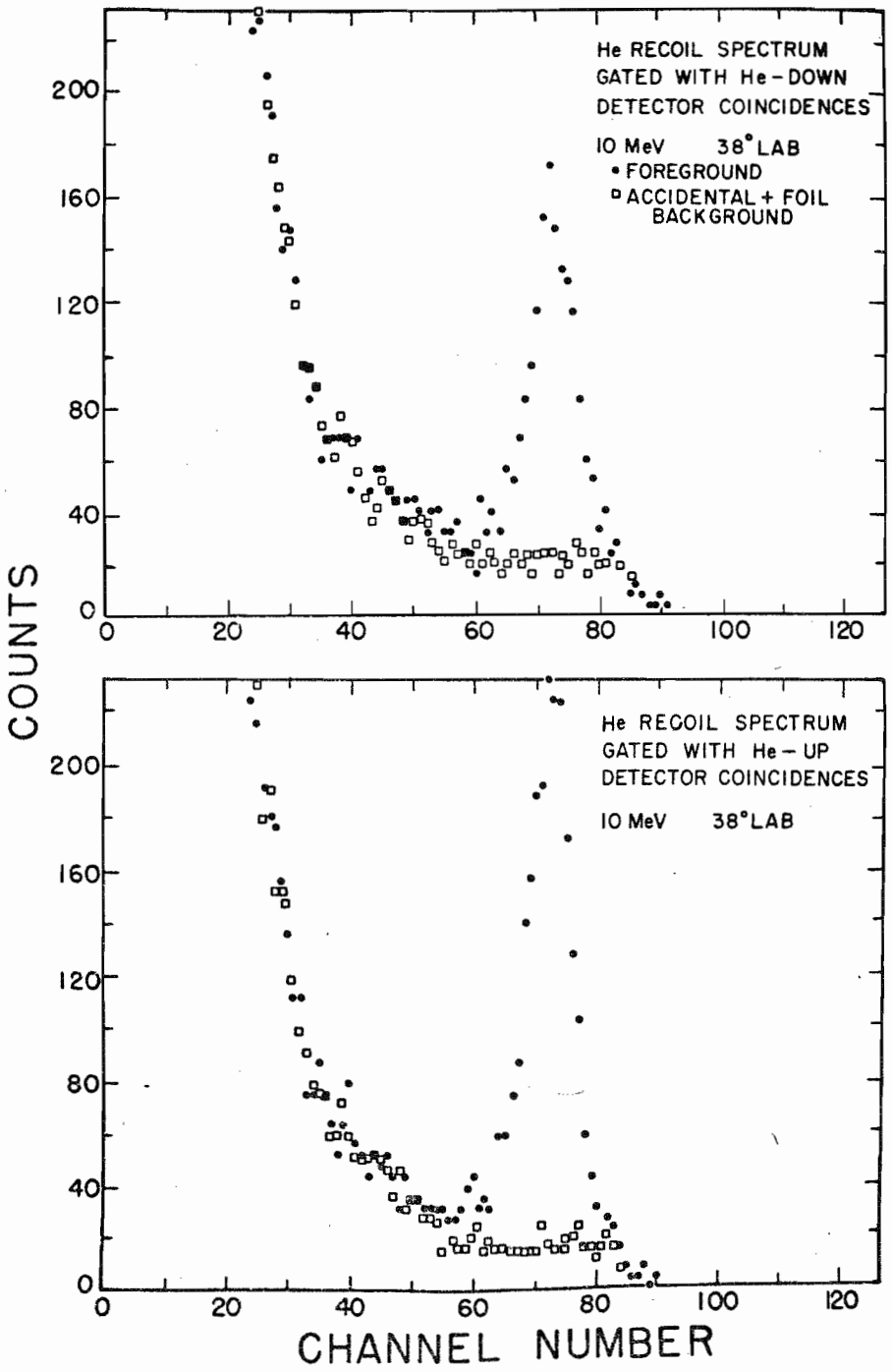
He RECOIL SPECTRUM
GATED WITH He – DOWN
DETECTOR COINCIDENCES
10 MeV 38° LAB
• FOREGROUND
□ ACCIDENTAL + FOIL
BACKGROUND
He RECOIL SPECTRUM
GATED WITH He – UP
DETECTOR COINCIDENCES
10 MeV 38° LAB
COUNTS
CHANNEL NUMBER
0
40
80
120
160
200
0
20
40
60
80
100
120

Figure 8. D(d,n) Sum Spectrum and Backgrounds

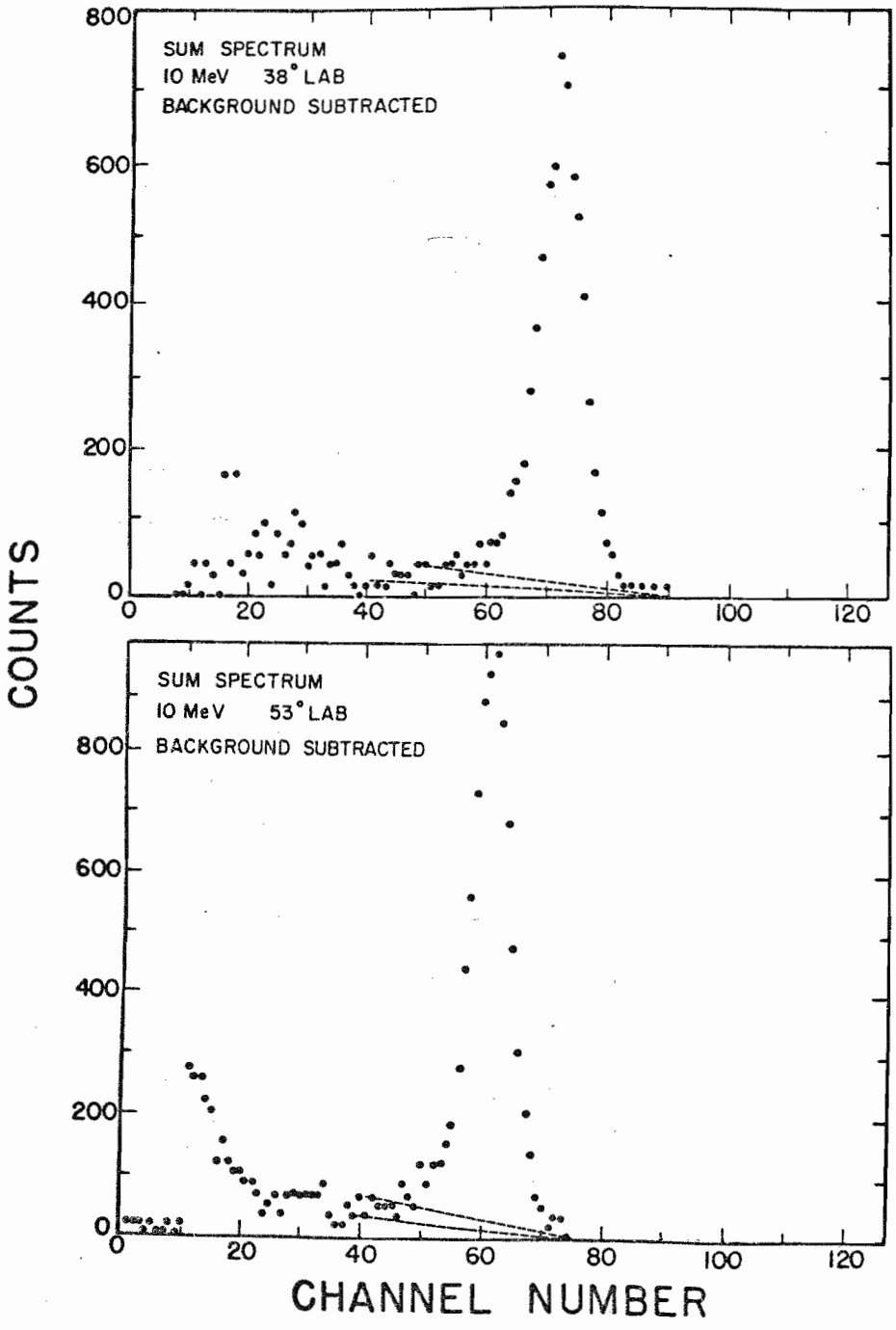
SUM SPECTRUM
10 MeV 38° LAB
BACKGROUND SUBTRACTED
SUM SPECTRUM
10 MeV 53° LAB
BACKGROUND SUBTRACTED
COUNTS
CHANNEL NUMBER
0
200
400
600
800
0
20
40
60
80
100
120

were used to compute the average analyzing power using the Monte-Carlo program MOCCASINS. The accuracy of this calculation did not introduce appreciable errors into the extracted polarization values.

C. A Further Finite Geometry Correction

A further correction was applied to the data. Due to the finite size of the He cell and the deuterium target, neutrons emitted in a range of reaction angles reach the polarimeter and are detected. Since the differential cross section and neutron polarization change rapidly with reaction angle, the average neutron polarization that the polarimeter sees can be somewhat different from the true polarization at the central polarimeter angle. Only a first order correction for this effect was applied to the data because the effect is small.

The correction was calculated in the following manner. The code POLN, described in a later chapter, was used to generate fits to the experimental polarization distributions. These smooth curves were then averaged (weighted by the differential cross section) over the deuterium target and the He cell dimensions. Thus new polarization distributions were obtained. Differences between these two distributions then represented a first order estimate of the target and He cell finite size effect and were therefore applied as corrections to the extracted experimental polarizations. These corrections were very small, the largest occuring at 12 MeV and 35^{o}(c.m.) having a magnitude of 0.0087.

D. Results

Experimental polarization distributions of the neutrons from the $D(d,n)^{3}He$ reaction were measured at deuteron energies of 6, 8, 10, 12, and

14 MeV. The results are exhibited in Figure 9 and listed in Table 1. They include some recent data obtained at our lab by Hardekopf (1971) at 18 MeV. The smooth curves through the data are discussed below. The data were obtained and are presented at center of mass angles smaller than ninety degrees since the distributions are anti-symmetric about 90°(c.m.)due to the identity of target and bombarding particles.

Curve fitting--According to Simon and Welton (1953) the differential cross section for a reaction can be expressed as a sum of Legendre polynomials of the form

$$\sigma(\theta) = \sum_{k=0}^{k=M} c_k P_k(\cos\theta)$$

The complexity rule (Blatt and Biedenharn, 1952) states that the value of the sum limit M can be no larger than twice the largest angular momentum contributing to the reaction. A similar expression in terms of the associated Legendre polynomials $P'_k(\cos\theta)$ can be written for the differential polarization distribution:

$$\pi(\theta) = P(\theta)\sigma(\theta) = \sum_{k=1}^{k=N} a_k P'_k(\cos\theta)$$

Again the upper limit on N is the same as on M above. Further, because of the identity of target and incident particles, a_k and c_k vanish for odd values of k.

A computer program POLN was written which can either generate differential cross sections from the a_k coefficients available in the literature or determine these coefficients from a least squares fit to cross

Figure 9. $D(d,n)^3He$ Polarization Angular Distributions

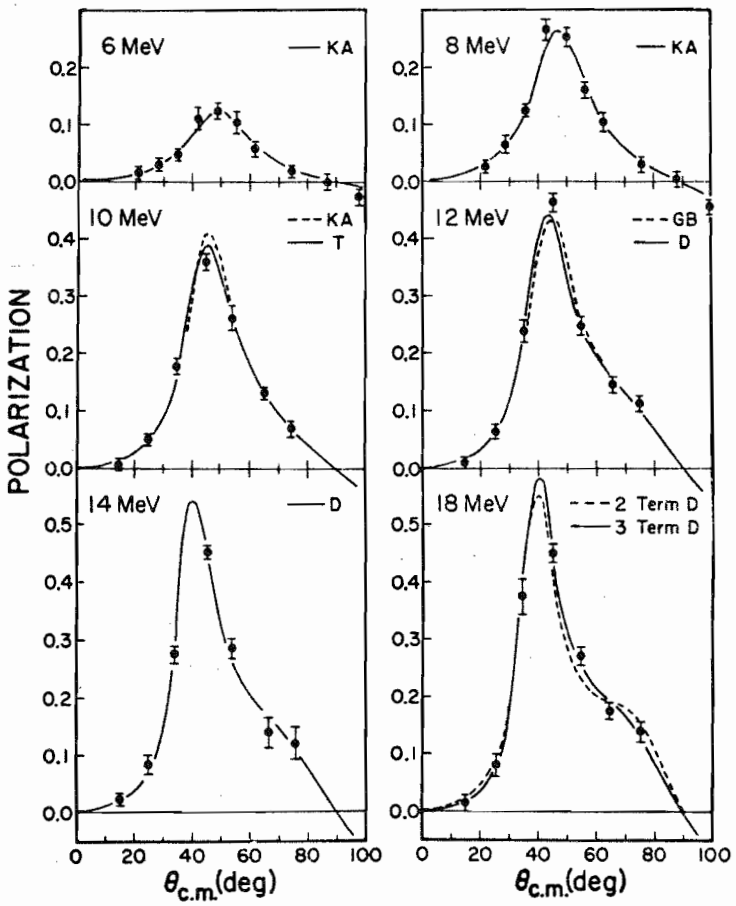
6 MeV
KA
8 MeV
KA
10 MeV
KA
T
12 MeV
GB
D
14 MeV
D
18 MeV
2 Term D
3 Term D
POLARIZATION
θc.m.(deg)
θc.m.(deg)

TABLE 1

Neutron Polarization Values for the $D(d,n)^3He$ Reaction

E_d(MeV)	$\theta_{c.m.}$ (deg)	E_N(MeV)	Polarization	Error
6.0	21.0	9.0	0.015	0.012
	27.9	8.8	0.030	0.008
	34.8	8.5	0.046	0.008
	41.6	8.3	0.111	0.017
	48.3	8.0	0.126	0.016
	55.0	7.6	0.105	0.019
	61.5	7.2	0.057	0.014
	74.2	6.5	0.019	0.010
	86.4	5.7	-0.001	0.013
	97.8	4.9	-0.025	0.014
8.0	21.4	10.8	0.027	0.009
	28.5	10.6	0.066	0.017
	35.5	10.3	0.126	0.012
	42.5	9.9	0.269	0.018
	49.3	9.5	0.254	0.017
	56.1	9.1	0.162	0.016
	62.8	8.6	0.107	0.018
	75.7	7.6	0.031	0.014
	88.0	6.6	0.006	0.014
	99.6	5.7	-0.044	0.016
10.0	14.5	12.9	0.007	0.010
	24.6	12.5	0.049	0.010
	34.6	12.0	0.178	0.015
	45.0	11.3	0.357	0.015
	54.2	10.7	0.262	0.023
	65.0	9.8	0.133	0.010
	74.2	9.0	0.071	0.014
12.0	14.7	14.7	0.010	0.009
	24.9	14.3	0.065	0.012
	35.0	13.7	0.232	0.018
	45.0	13.0	0.457	0.015
	54.8	12.2	0.249	0.017
	65.7	11.1	0.146	0.015
	75.0	10.1	0.113	0.014

Table 1-Continued

E_d(MeV)	$\theta_{c.m.}$ (deg)	E_N(MeV)	Polarization	Error
14.0	14.8	16.6	0.022	0.011
	25.1	16.1	0.084	0.019
	33.9	15.4	0.268	0.015
	45.0	14.6	0.444	0.012
	53.8	13.6	0.284	0.017
	66.3	12.4	0.139	0.032
	75.6	11.3	0.119	0.030
18.0	15.0	20.2	0.014	0.014
	25.4	19.7	0.081	0.019
	34.3	19.0	0.376	0.031
	45.0	17.9	0.450	0.016
	54.5	16.7	0.272	0.016
	64.3	15.4	0.177	0.015
	75.2	13.8	0.141	0.018

section data. It also generates differential polarization distributions by multiplying the experimental polarization by these calculated cross sections. In addition it can also determine the a_k coefficients by least squares fitting of the above differential polarization distributions and then calculate smooth polarization curves.

For completeness, Figure 10 shows the differential polarizations at 1.5, 1.9, 3.0, and 3.7 MeV formed from the $P(\theta)$ values of Purser (1966) and the $\sigma(\theta)$ values of Fowler and Brolley (1960). Figure 11 shows similar distributions for the present data and that of Hardekopf (1971) at 18 MeV. The c_k coefficient sets used in generating the latter distributions were those of Kerr and Anderson (1968), Thornton (1969), Dietrich et al. (1970), Goldberg and LeBlanc (1960), and Brolley et al. (1957). Labels for these sets are KA, T, D, GB, and BPR respectively. Statistical errors for the c_k coefficients were quoted only by Thornton although Dietrich et al. estimate 5% uncertainties. Uncertainties of 0.3 were assigned to all the available c_k coefficients. They represent a compromise value based on the uncertainties of Thornton and the discrepancies between coefficient sets available at the same energies. Fits to $\pi(\theta)$ using two, three and four a_k coefficients were performed on the data (solid lines, Figure 11). Including the a_6 coefficient improved the fit appreciably only at 14 MeV and 18 MeV. At energies below 14 MeV its inclusion did not affect the fits and, when extracted, its value was consistent with zero. Discrepancies in the $\pi(\theta)$ fits at 10 MeV using KA and T $\sigma(\theta)$ coefficients and at 12 MeV using the GB and D $\sigma(\theta)$ coefficients did not produce large differences in the calculated polarizations (Figure 9). Table 2 lists the results of the three coefficient fits and the sources of the $\sigma(\theta)$ coefficients. The energy dependence of all the extracted

Figure 10. $D(d,n)^3He$ Differential Polarization Distributions-Purser

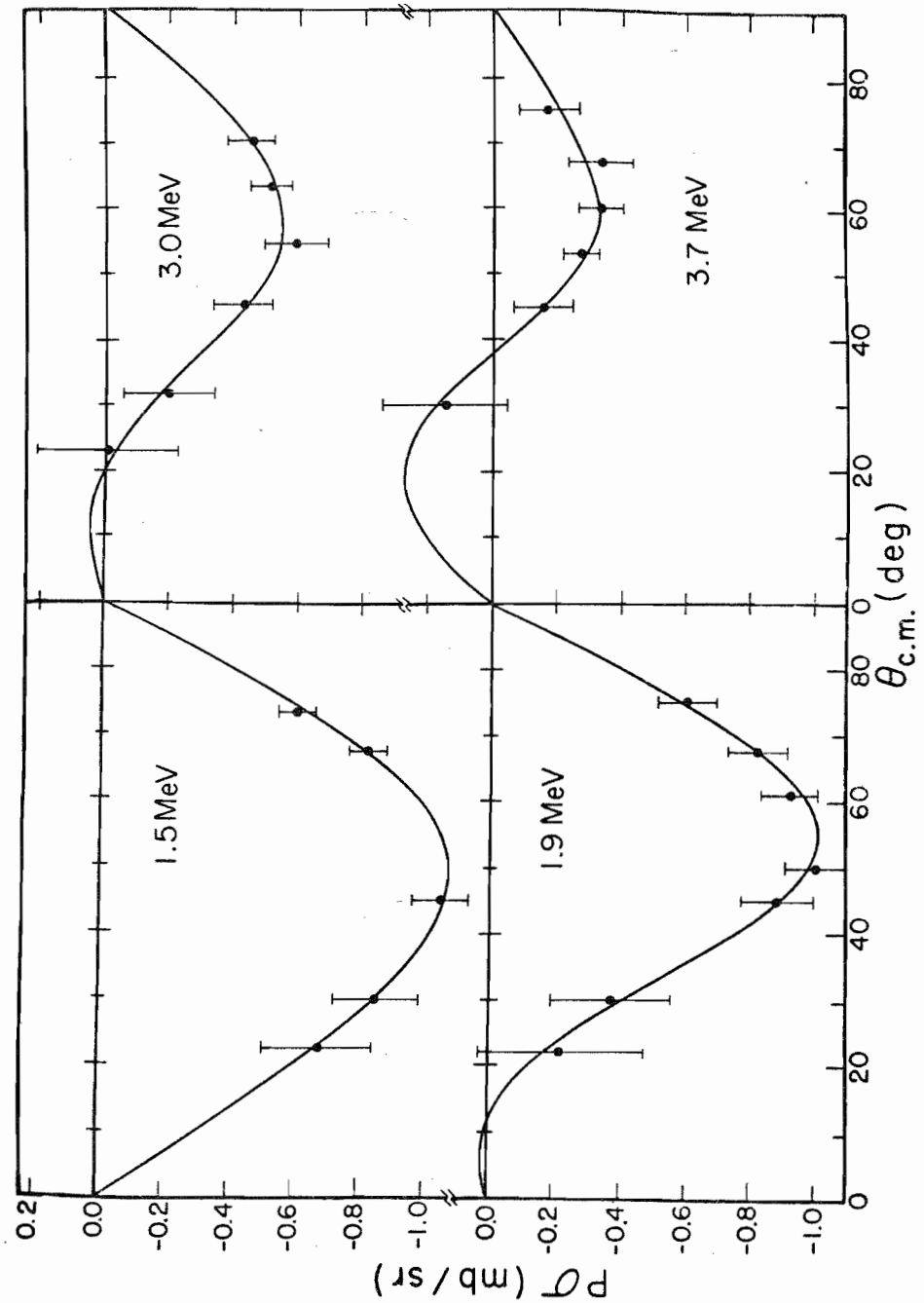
3.0 MeV
1.5 MeV
3.7 MeV
1.9 MeV
pσ (mb/sr)
θc.m. (deg)
0.2
0.0
-0.2
-0.4
-0.6
-0.8
-1.0
0
20
40
60
80

Figure 11. $D(d,n)^3He$ Differential Polarization Distributions

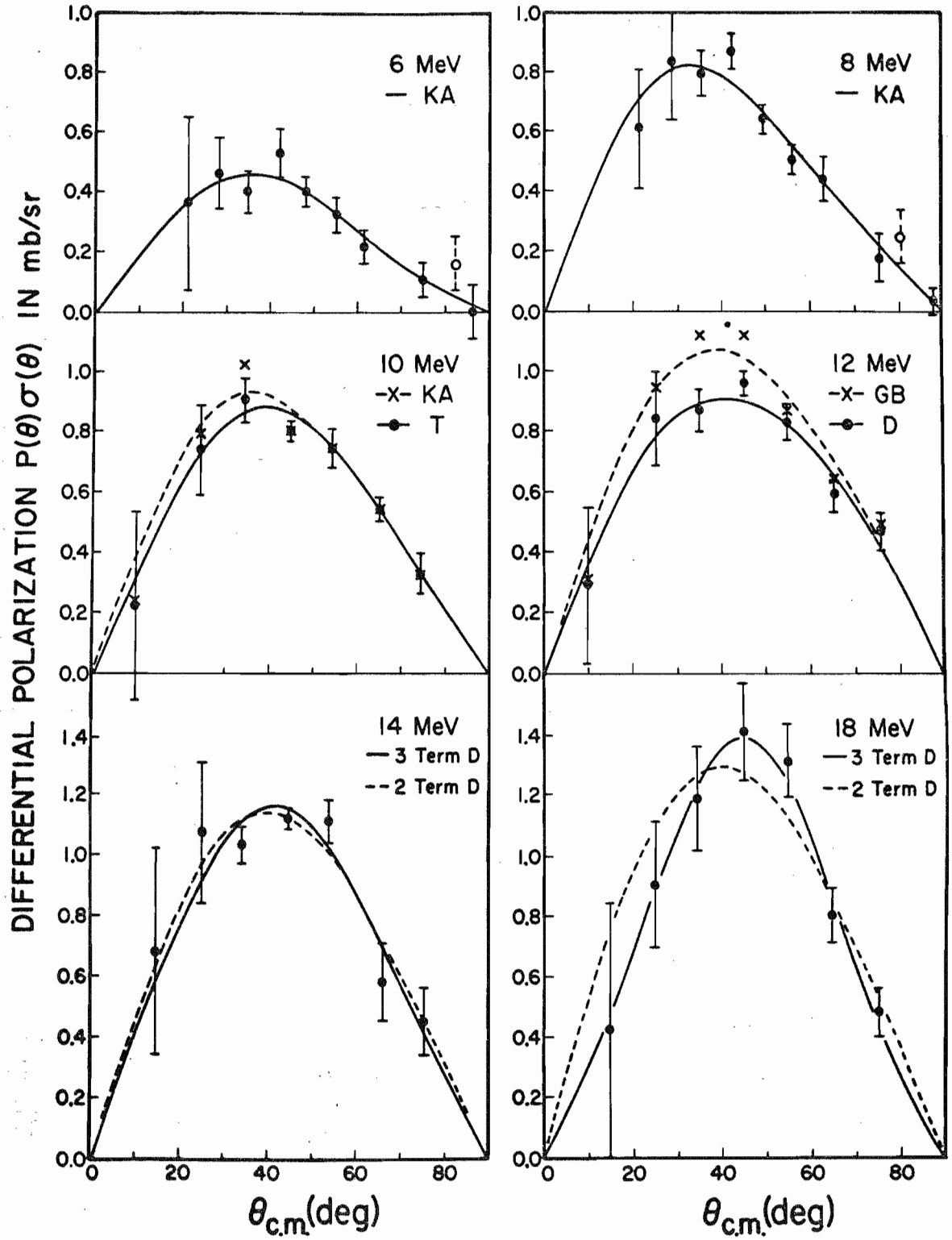
6 MeV
— KA
8 MeV
— KA
10 MeV
-x- KA
— T
12 MeV
-x- GB
— D
14 MeV
— 3 Term D
--2 Term D
18 MeV
— 3 Term D
--2 Term D
DIFFERENTIAL POLARIZATION P(θ)σ(θ) IN mb/sr
θc.m.(deg)
θc.m.(deg)

TABLE 2

Coefficients of Associated Legendre Polynomial Expansion for $\pi(\theta)$

E_d (MeV)	a_2	a_4	a_6	Reference for $\sigma(\theta)$ Coefficients
1.5	-0.72 ± 0.04	0.04 ± 0.02	0.01 ± 0.02	FB
1.9	-0.58 ± 0.04	0.13 ± 0.03	0.02 ± 0.02	FB
3.0	-0.30 ± 0.03	0.10 ± 0.03	0.02 ± 0.02	FB
3.7	-0.10 ± 0.04	0.11 ± 0.04	0.03 ± 0.03	FB
6.0	0.23 ± 0.02	0.04 ± 0.02	-0.00 ± 0.01	T
	0.25 ± 0.02	0.05 ± 0.02	-0.00 ± 0.02	KA
8.0	0.43 ± 0.03	0.08 ± 0.02	0.01 ± 0.02	BPR
	0.46 ± 0.03	0.08 ± 0.02	0.01 ± 0.02	KA
10.0	0.55 ± 0.03	0.05 ± 0.02	-0.01 ± 0.02	T
	0.55 ± 0.03	0.05 ± 0.02	-0.01 ± 0.02	BPR
	0.57 ± 0.03	0.07 ± 0.02	0.00 ± 0.02	KA
12.0	0.68 ± 0.04	0.05 ± 0.03	0.01 ± 0.03	GB
	0.61 ± 0.04	0.03 ± 0.03	0.01 ± 0.02	BPR
	0.60 ± 0.04	0.02 ± 0.03	0.01 ± 0.02	D
14.0	0.72 ± 0.04	0.05 ± 0.03	-0.02 ± 0.03	D
18.0	0.82 ± 0.04	0.03 ± 0.03	-0.06 ± 0.03	D

coefficients is shown in Figure 12 . Good agreement is evident between the a_k coefficients extracted using different c_k coefficient sets.

Contrary to expectations, the number of coefficients needed to fit the differential polarization is not the same as that needed for the $\sigma(\theta)$ fits as allowed by the complexity rule.

No special conclusion is drawn from this fact since it could be the result of fitting a small number of $P(\theta)$ data whose uncertainties are larger than those of the $\sigma(\theta)$ data alone. The same phenomenon occurs in the D(d,p)T data of Porter and Haeberli (1967) and the Hardekopf (1971) data.

It should be mentioned that the same fitting procedure was used on the data before the correction for the finite size of the target and He cell was applied. The coefficients from that fit were used, as described in a previous section, to compute a first order correction for this effect.

E. Comparison with D(d,p) Data

As exhibited in the previous section the D(d,n)^{3}He polarization peaks near 45^o(cm.), the maximum moving to smaller angles as the bombarding energy is increased. When a comparison is made between the present data near 45^o(cm) with those of Alekseev et al. (1964), May et al. (1963), Babenko et al. (1965), Niewodniczanski et al. (1964), and Dubbeldam and Walter (1961), the agreement between these data sets extends to approximately 10 MeV (Figure 13). However at 12 and 14 MeV the present data shows a polarization approximately 1.5 times larger than that of Dubbeldam and Walter and that of Alekseev. The D(d,n) data of Hardekopf at 18 MeV exhibits a polarization approximately twice as large as that reported by Alekseev at this energy. The larger polarization values at these energies decrease the differences between the D(d,n) and D(d,p) polarizations.

Figure 12. Energy Dependence of Differential Polarization Coefficients

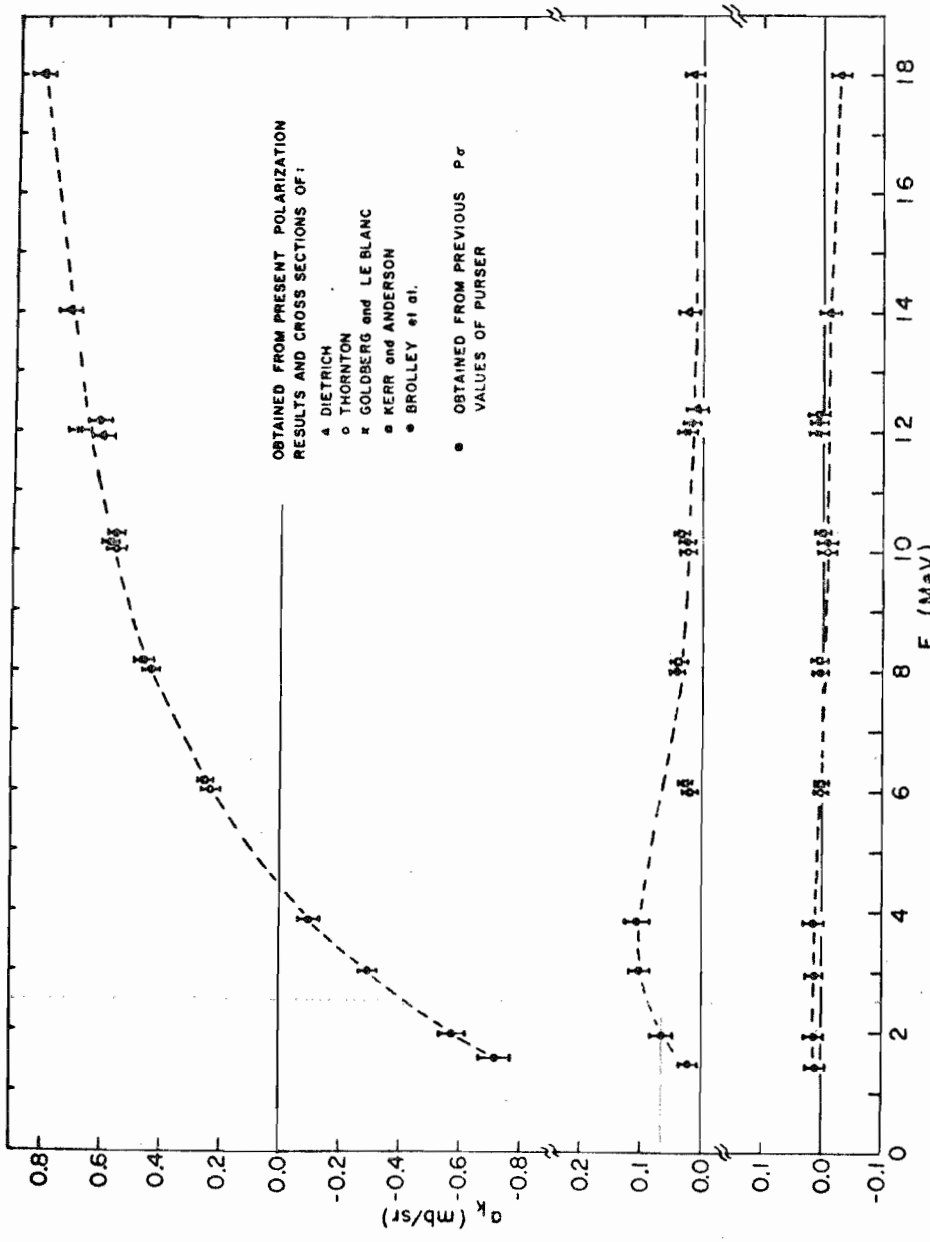
OBTAINED FROM PRESENT POLARIZATION RESULTS AND CROSS SECTIONS OF:
▲ DIETRICH
○ THORNTON
× GOLDBERG and LE BLANC
■ KERR and ANDERSON
● BROLLEY et al.
● OBTAINED FROM PREVIOUS Pσ VALUES OF PURSER
σ_K (mb/sr)
E_d (MeV)

Figure 13. $D(d,n)^3He$ Comparison with Earlier Data at $\sim 45^{o}$ c.m.

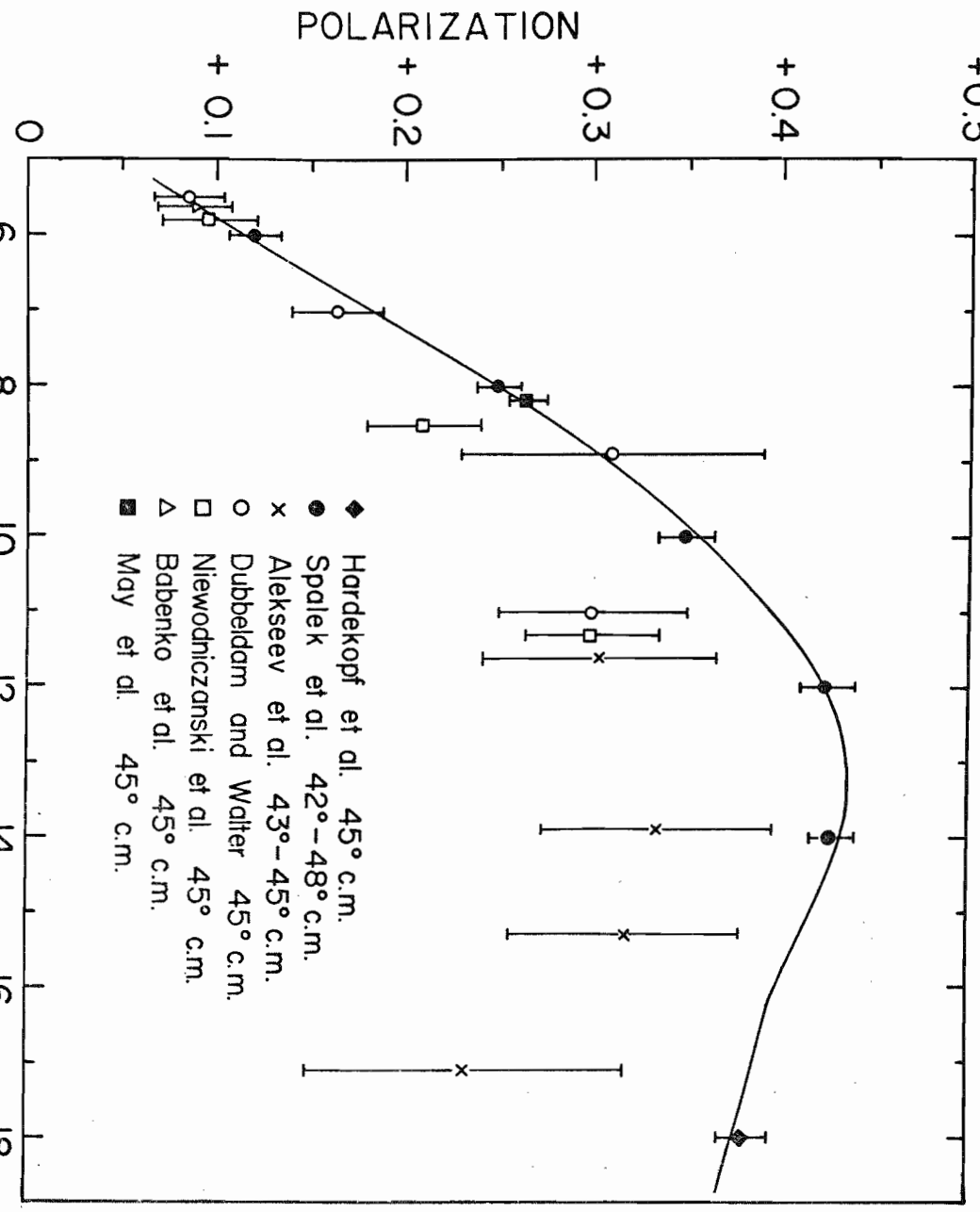
POLARIZATION
+0.5
+0.4
+0.3
+0.2
+0.1
0
6
8
10
12
14
16
18
E_d (MeV)
Hardekopf et al. 45° c.m.
Spalek et al. 42°-48° c.m.
Alekseev et al. 43°-45° c.m.
Dubbeldam and Walter 45° c.m.
Niewodniczanski et al. 45° c.m.
Babenko et al. 45° c.m.
May et al. 45° c.m.

The recent D(d,p)T data of Hardekopf (1971) accumulated at the same energies as the present data are compared with the latter in Figure 14 . This comparison shows a discrepancy of large magnitude between the neutron and proton polarizations in the energy range 6.0 to 10.0 MeV. The neutron polarization is consistently lower with the largest differences occuring near 45^{o}(c.m.),i.e. near the differential cross section minimum. These differences decrease with increasing energy, the effect being still present at 12 MeV. However, at 14 MeV the proton and neutron polarization values are too close compared to the data uncertainties to make a definite statement about their relative magnitudes. Thus it is considered established that real differences between the polarizations in these reactions do indeed exist but that they are smaller than suggested by earlier work and that they decrease with increasing deuteron energy. Furthermore, the D(d,n)^{3}He reaction holds promise as a source of polarized neutrons despite some of the drawbacks discussed in the next section.

F. Conclusions

The threshold energy for the deuteron break-up reaction D(d,np)D is 4.45 MeV. Neutrons from this process are then present, as well as the D(d,n) neutrons, when this reaction is used at the energies considered here. The yield of break-up neutrons rises rapidly with increasing deuteron energy (Cranberg et al., 1956) from a 0^{o} value of 11.4 mb/sr at 6.21 MeV to 32.0 mb/sr at 7.33 MeV and reaches 80 mb/sr at 18.8 MeV (Rybakov et al., 1961) deuteron energy. The relative separation in energy of the break-up neutron spectrum and the monoenergetic D(d,n) neutrons at any reaction angle decreases with energy, making their separation difficult. The ability to identify these

Figure 14. Comparisons of D(d,p)T and $D(d,n)^3He$ Polarizations

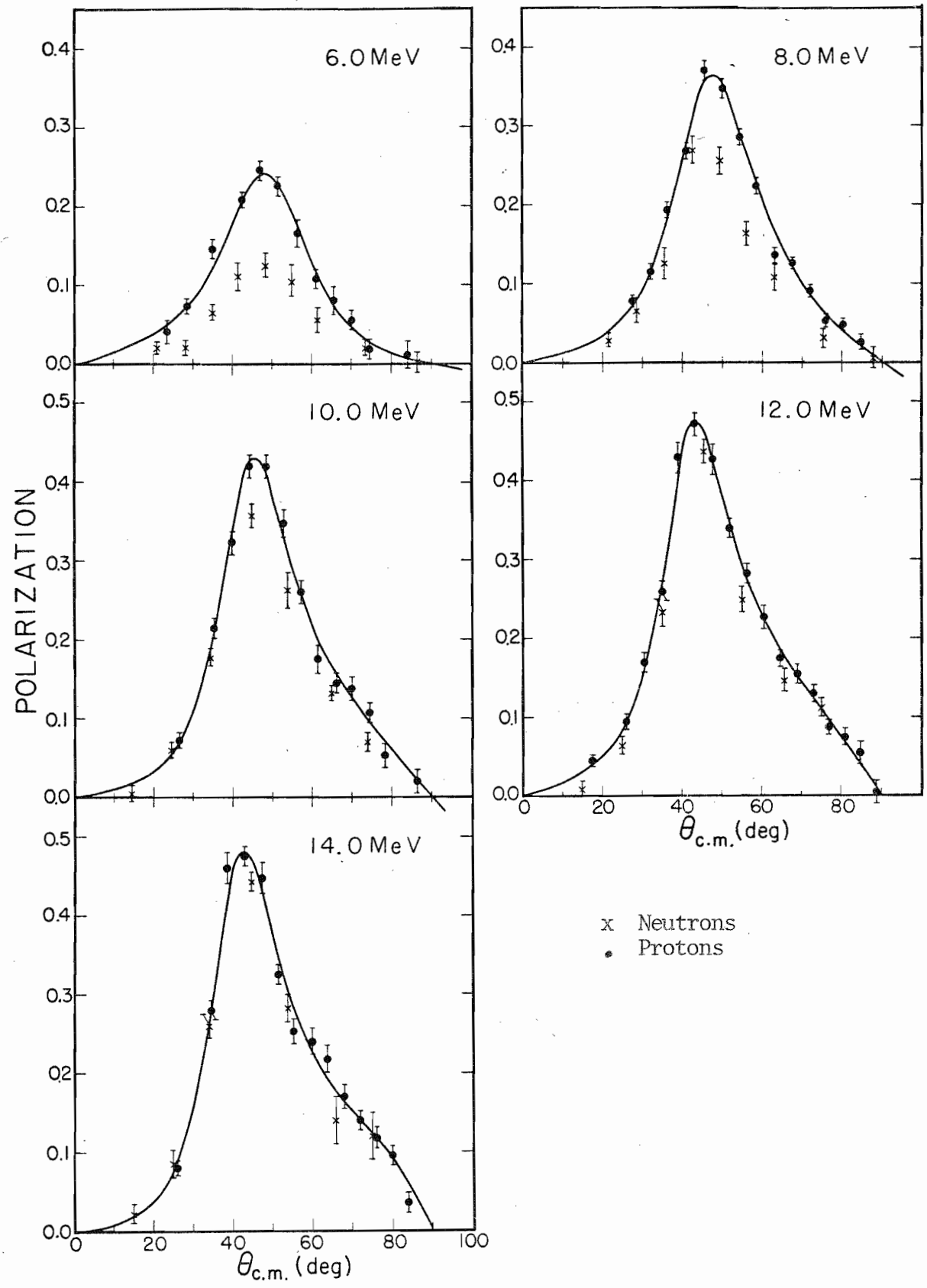
6.0 MeV
8.0 MeV
10.0 MeV
12.0 MeV
14.0 MeV
POLARIZATION
θc.m. (deg)
x Neutrons
• Protons

neutrons is important if the D(d,n) reaction is to be a useful source of polarized neutrons. At about 45^{o}(c.m) the cross sections for the D(d,np) and D(d,n) reactions are of the same order of magnitude so their separation is essential at this angle where $P(\theta)$ has its highest (and most useful) value. Energy degraded neutrons produced when the very high forward neutron flux scatters from the laboratory walls and floor also contribute some background at this angle. As shown by this experiment, separation of these groups would be possible with techniques similar to the present ones. Also, although the highest polarization values occur at minima in the differential cross section, large target thicknesses are available with low beam energy losses. The only other reactions producing monoenergetic highly polarized neutrons in the energy range of 8 to 15 MeV are the $T(d,n)^{4}He$ and the $T(p,n)^{3}He$ reactions (Walter, 1970). However, since the Q value of the T(d,n) reaction is +14 MeV, this source cannot be used to obtain polarized neutrons below this energy. Besides the fact that a tritium beam or target presents a radiation hazard, the T(p,n) reaction is inferior to the D(d,n) reaction as a source of polarized neutrons due to the high proton energies needed. To produce neutrons of high polarization in the energy range 8 to 15 MeV the proton energies required are 10.5 to 19 MeV. These energies are available by the use of only the latest tandem accelerators or cyclotrons. Thus, the D(d,n) reaction, despite the drawbacks mentioned earlier is the best source of highly polarized 8 to 15 MeV neutrons.

The evaluation of the energy dependence and magnitudes of the differences between the D(d,n) and D(d,p) polarization distributions is difficult. Coulomb effects being responsible is suggested by the decrease in these differences with increasing energy. Yet the bombarding energies and large positive Q values (high outgoing channel energies) are large

compared to the d-d and d-p Coulomb barriers. Under these conditions very small Coulomb effects would be expected. The lack of a theoretical model for this reaction prevents making an estimate of the Coulomb effects to be expected in these reactions at the energies studied. Estimates of these effects cannot be made with present DWBA codes because the identity of the particles requires symmetrization of the wave functions and the codes are of very dubious value for light projectiles and targets because of the assumptions inherent in them. An attempt at applying the DWBA to the present situation would thus represent a major effort and was not considered worth the time in view of the expected low value of the results. No statement can therefore be made that the observed differences are due to violation of the charge symmetry of nuclear forces, however this possibility is not ruled out. It is hoped that such a possibility will encourage theoretical work in this area, especially in view of the importance the possible symmetry violation would have in understanding nuclear interactions.

Chapter V

^{9}Be(d,n) DATA HANDLING AND RESULTS

A. Data Acquisition

Again, as in the D(d,n) case, the solenoid was cycled at regular integrated charge intervals. The same electronics warm-up, detector count rate monitoring, and detector efficiency monitoring procedures were also followed. However, the solenoid current was set to precess by 90^{o} the spin of a neutron whose energy was midway between the n_0 and n_3 group energies. This kept the spin precession correction factor SPCF for all groups from becoming too large with the resultant increase in the polarization uncertainties.

B. Analysis of Spectra

The Fortran program PROMETHEUS described extensively by Thomason (1969) was used to analyze the ^{9}Be(d,n) data. It was because of the previous success in stripping down data with this type of fitting program that the ^{9}Be(d,n) experiment was feasible. Only the features of interest for this work will be described. In the program, the experimental spectra are corrected for accidental backgrounds and assigned the array names UP(I), DP(I), UM(I), and DM(I) where I is the channel number. Two new spectra, EXPR(I) and

EXPL(I), are formed from the products $(UP(I)*DM(I))^{\frac{1}{2}}$ and $(UM(I)*DP(I))^{\frac{1}{2}}$ respectively, corresponding to UP and DOWN spectra. A third spectrum EXPSPC(I) = EXPR(I) + EXPL(I) is also calculated as well as a spectrum of the associated statistical errors for each of the above spectra.

The sum spectrum EXPSPC(I) is then represented by a sum of gaussians of the form:

$$SPCTOT(I) = \sum_{J=1}^{NEN} AMP(J) \cdot EXP(-((E(I)-EN(J))/(RES(J)\cdot EN(J)))*2)$$

where AMP(J), EN(J), and RES(J) are the amplitude, neutron energy, and resolution, respectively, for the Jth neutron group and I is the channel number.

After the initial estimates of the free parameters are input, SPCTOT(I) and EXPSPC(I) are compared and χ^2 is calculated. The Gauss linear least squares method is used to vary the parameters to minimize χ^2. The new parameters resulting from the iterative χ^2 search are output along with plots of the experimental spectrum and the best fit to it.

Similar searches can be conducted to fit the EXPR(I) and EXPL(I) spectra. The amplitudes of the gaussians from these fits are then used to compute the asymmetries for the individual neutron groups. Again the spectra and the fits can be output along with experimental and calculated channel by channel asymmetries and their errors.

The flexibility of the program will become apparent when the analysis procedure followed in the present work is described below. Figure 15 shows a typical sum EXPSPC(I) spectrum (dots) and the best fit (dashes) which is composed of the sum of 6 gaussians (solid lines). The most energetic neutron group (n_o) is represented by the gaussian furthest to the right with corresponding gaussians for the other groups.

Figure 15. $^{9}Be(d,n)$ Sum Spectrum

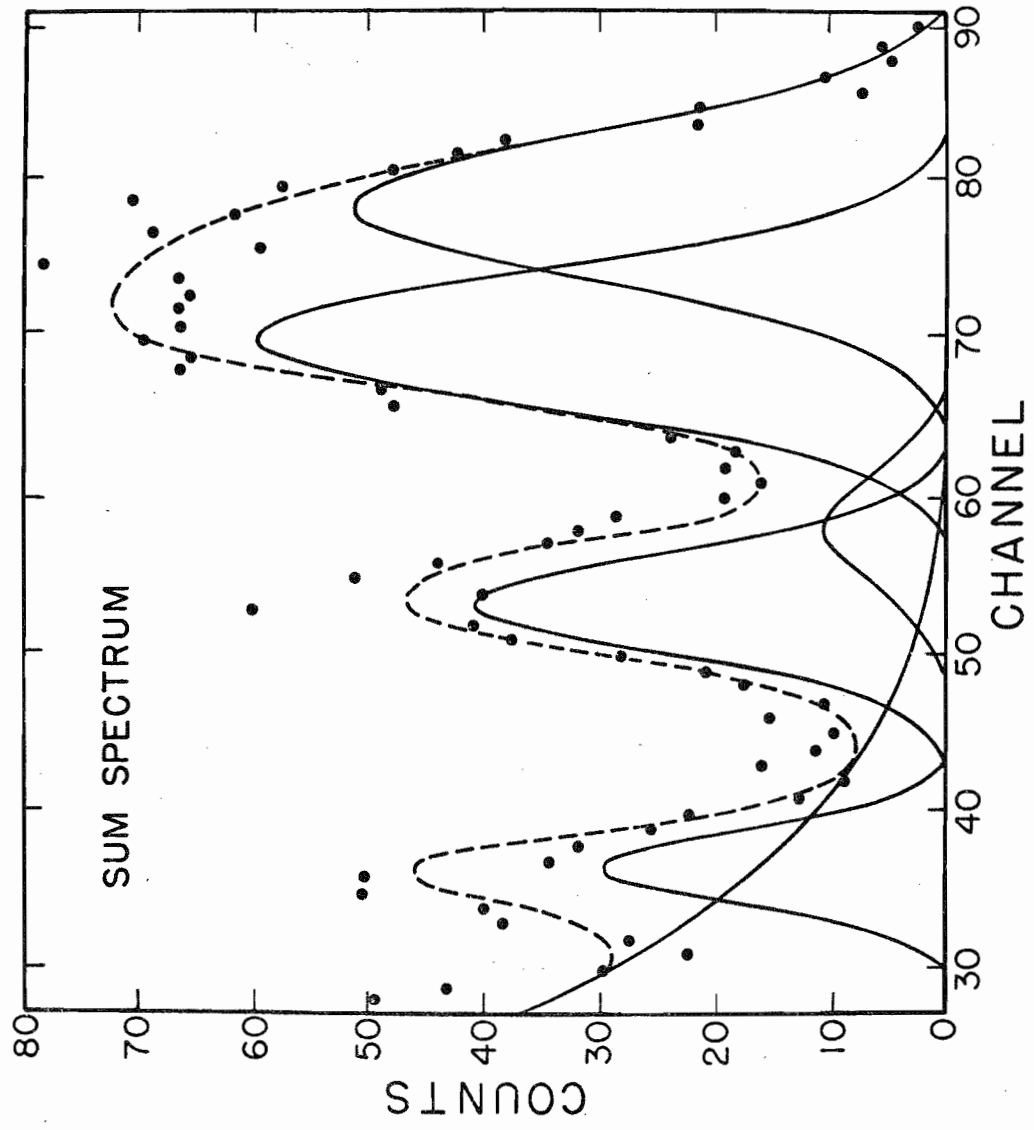
SUM SPECTRUM
COUNTS
CHANNEL
0
10
20
30
40
50
60
70
80
30
40
50
60
70
80
90

Initial estimates of the amplitudes of the 5 gaussians and the energy to channel number scale factor CHE were made. Since the helium cell and associated electronics are linear, a determination of CHE automatically centers the n_o to n_4 group gaussians at the proper channels once their energies are input. The resolution of the polarimeter for each group was calculated according to the formula of Morgan (1968):

$$RES(J) = SQRT(ARES + BRES/EN(J))$$

where the resolution parameters ARES and BRES were determined from the line shapes of $^{12}C(d,n)$ spectra accumulated during the solenoid calibrations at different energies. Their values were ARES = 0.016 and BRES = 0.020, giving a resolution of about 14% for the neutron energies in question. A sixth gaussian, whose parameters were adjusted independently, was used to simulate the background under the n_4 peak. Its EN(J) was fixed at -0.5 MeV.

The chosen search combinations for the sample spectra in Figures 15 and 16 were: a) channels 25 to 90 of the EXPSPC(I) were fit with all amplitudes and CHE as free parameters; b) because the n_o to n_3 groups were too close to be isolated, the n_4 group was next used to determine the final CHE value. Channels 30-40 were fit with AMP(6), RES(6), and CHE as free parameters using the results of a) as initial estimates; c) with CHE and RES(6) fixed, channels 30-90 were fit, all amplitudes being varied; d) next, a search on channels 30-90 of the UP and DOWN spectra (Figure 16) was performed with all amplitudes free except that of the background gaussian which was well determined from the sum spectrum fits. Experimental and calculated channel by channel asymmetries were compared to check the quality of the fit.

Figure 16. ^{9}Be(d,n) 'UP' and 'DOWN' Spectra

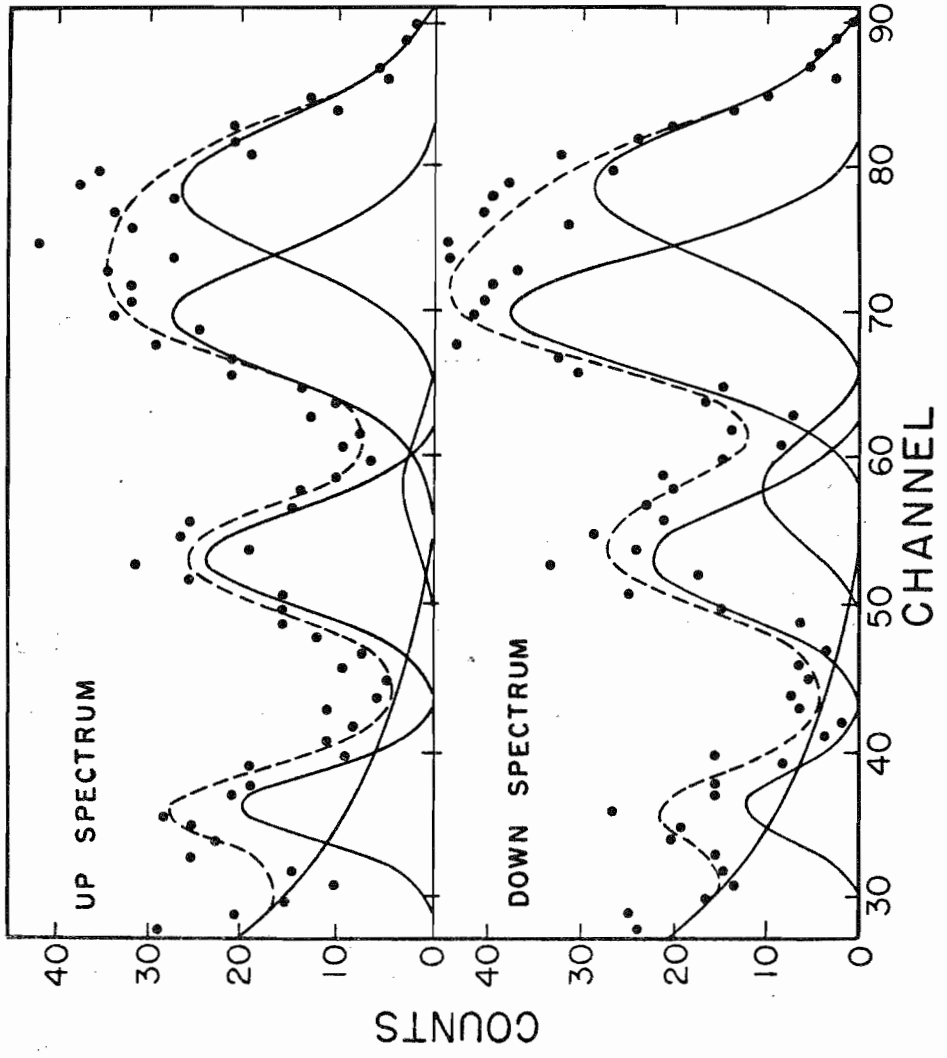
UP SPECTRUM
DOWN SPECTRUM
COUNTS
CHANNEL
0
10
20
30
40
30
40
50
60
70
80
90

Two methods were used to check the validity of this fitting procedure. An "all amplitudes and CHE free" search on the sum spectrum followed by an UP-DOWN amplitudes-free search were performed. Also, at angles where the relative cross sections of the neutron groups were available a similar search was conducted. The constraint imposed was that the amplitude ratios n_o/n_1 and n_2/n_3 be fixed according to the corresponding cross section ratios. These three fitting methods produced results that agreed within the statistical error limits. The values quoted later are based mainly on procedure a) to d) which was felt to be the most accurate method of determination.

C. Results and Discussion

Spin correction factors were calculated from the solenoid currents, neutron energies, and solenoid calibration as described in Chapter II. Values of the average analyzing power $\overline{P}_2$ derived by Thomason (1969) from the n-He phase-shifts of Satchler (1968) were used to extract polarizations from the data. These values of $\overline{P}_2$ included the effects of polarimeter geometry, the variation of organic scintillator efficiencies with energy, and double scattering in the He cell.

The results for 3 and 3.5 MeV deuteron energies are presented in Table 3 and the polarization results are plotted in Figure 17. In Table 3, EO, THL, THCM, GRP, and EN are the laboratory deuteron energy, laboratory reaction angle, center of mass reaction angle, neutron group, and neutron energy respectively.

The errors in the n_2 group data are very large because overlap of the low intensity n_2 group with the n_1 and n_3 groups in the gated recoil spectra (see Figure 15) introduced large errors in the n_2 amplitude

TABLE 3

Neutron Polarization Values for the $^{9}Be(d,n)^{10}B$ Reaction

EO	THL	GRP	THCM	EN	Polarization
3.00	-30.0	N0	-32.6	7.2	0.08 ± 0.05
		N1	-32.7	6.5	-0.09 ± 0.04
		N2	-33.0	5.5	0.09 ± 0.09
		N3	-33.1	5.1	-0.06 ± 0.05
		N4	-33.7	3.6	-0.01 ± 0.05
	10.0	N0	10.9	7.3	-0.19 ± 0.07
		N1	11.0	6.6	-0.02 ± 0.04
		N2	11.0	5.6	-0.12 ± 0.09
		N3	11.1	5.2	0.06 ± 0.08
		N4	11.3	3.7	0.09 ± 0.05
	20.0	N0	21.8	7.3	-0.22 ± 0.10
		N1	21.9	6.6	0.03 ± 0.04
		N2	22.0	5.6	-0.21 ± 0.13
		N3	22.1	5.1	-0.08 ± 0.07
		N4	22.6	3.7	0.17 ± 0.07
	30.0	N0	32.6	7.2	-0.12 ± 0.06
		N1	32.7	6.5	-0.01 ± 0.04
		N2	33.0	5.5	-0.09 ± 0.13
		N3	33.1	5.1	0.01 ± 0.06
		N4	33.7	3.6	0.10 ± 0.05
	40.0	N0	43.3	7.1	-0.02 ± 0.06
		N1	43.5	6.4	0.17 ± 0.04
		N2	43.8	5.4	-0.23 ± 0.26
		N3	44.0	5.0	0.10 ± 0.05
		N4	44.8	3.5	0.21 ± 0.09
	50.0	N0	53.9	6.9	0.00 ± 0.06
		N1	54.2	6.2	0.21 ± 0.05
		N2	54.6	5.2	0.28 ± 0.26
		N3	54.8	4.8	-0.00 ± 0.05
		N4	55.7	3.4	-0.03 ± 0.09
	60.0	N0	64.4	6.7	-0.06 ± 0.04
		N1	64.7	6.0	0.27 ± 0.03
		N2	65.1	5.1	-0.26 ± 0.22
		N3	65.4	4.7	0.13 ± 0.03
		N4	66.4	3.3	0.04 ± 0.05

Table 3-Continued

EO	THL	GRP	THCM	EN	Polarization
3.00	70.0	N0	74.8	6.5	0.02 ± 0.05
		N1	75.1	5.9	0.15 ± 0.05
		N2	75.6	4.9	-0.25 ± 0.21
		N3	75.8	4.5	0.07 ± 0.05
		N4	77.0	3.2	-0.04 ± 0.07
	85.0	N0	90.1	6.2	-0.07 ± 0.06
		N1	90.4	5.6	0.00 ± 0.05
		N2	90.9	4.6	-0.84 ± 0.36
		N3	91.2	4.3	0.11 ± 0.05
		N4	92.4	3.0	-0.59 ± 0.11
	100.0	N0	105.0	6.0	-0.05 ± 0.04
		N1	105.3	5.3	-0.18 ± 0.06
		N2	105.8	4.4	-0.32 ± 0.13
		N3	106.1	4.0	0.13 ± 0.08
		N4	107.3	2.8	0.17 ± 0.14
	115.0	N0	119.7	5.7	0.04 ± 0.05
		N1	119.9	5.1	-0.16 ± 0.04
		N2	120.4	4.2	-0.30 ± 0.23
		N3	120.6	3.8	0.06 ± 0.06
		N4	121.7	2.6	-0.10 ± 0.09
	125.0	N0	129.2	5.5	0.03 ± 0.06
		N1	129.4	4.9	-0.19 ± 0.06
		N2	129.9	4.0	-0.12 ± 0.21
		N3	130.1	3.7	0.01 ± 0.06
		N4	131.1	2.5	-0.19 ± 0.08
	135.0	N0	138.6	5.4	0.07 ± 0.07
		N1	138.8	4.8	-0.10 ± 0.05
		N2	139.2	3.9	-0.31 ± 0.31
		N3	139.4	3.6	0.15 ± 0.05
		N4	140.3	2.4	-0.20 ± 0.07
3.50	-30.0	N0	32.7	7.7	0.20 ± 0.05
		N1	32.8	7.0	-0.08 ± 0.04
		N2	33.1	5.9	-0.14 ± 0.12
		N3	33.2	5.5	0.03 ± 0.05
		N4	33.8	4.1	-0.02 ± 0.04

Table 3-Continued

EO	THL	GRP	THCM	EN	Polarization
3.50	10.0	N0	10.9	7.8	-0.40 ± 0.09
		N1	11.0	7.1	-0.06 ± 0.03
		N2	11.1	6.1	-0.04 ± 0.11
		N3	11.1	5.7	-0.02 ± 0.05
		N4	11.3	4.2	-0.00 ± 0.03
	20.0	N0	21.9	7.8	-0.30 ± 0.07
		N1	22.0	7.1	-0.05 ± 0.02
		N2	22.1	6.0	-0.01 ± 0.10
		N3	22.2	5.6	-0.04 ± 0.05
		N4	22.6	4.2	0.03 ± 0.03
	30.0	N0	32.7	7.7	-0.14 ± 0.05
		N1	32.8	7.0	-0.02 ± 0.03
		N2	33.1	5.9	0.06 ± 0.10
		N3	33.2	5.5	0.01 ± 0.05
		N4	33.8	4.1	-0.04 ± 0.03
	40.0	N0	43.5	7.5	-0.15 ± 0.09
		N1	43.6	6.8	0.16 ± 0.04
		N2	44.0	5.8	0.21 ± 0.14
		N3	44.1	5.4	-0.11 ± 0.07
		N4	44.9	4.0	0.02 ± 0.04
	50.0	N0	54.1	7.4	-0.01 ± 0.07
		N1	54.3	6.7	0.23 ± 0.04
		N2	54.7	5.7	0.18 ± 0.22
		N3	54.9	5.3	-0.01 ± 0.05
		N4	55.8	3.9	-0.03 ± 0.04
	60.0	N0	64.7	7.2	0.14 ± 0.07
		N1	64.9	6.5	0.18 ± 0.04
		N2	65.3	5.5	-0.20 ± 0.39
		N3	65.6	5.1	0.00 ± 0.04
		N4	66.5	3.7	-0.09 ± 0.04
	70.0	N0	75.1	6.9	0.03 ± 0.04
		N1	75.3	6.3	0.28 ± 0.09
		N2	75.8	5.3	-0.26 ± 0.32
		N3	76.0	4.9	-0.05 ± 0.04
		N4	77.1	3.6	-0.08 ± 0.03

Table 3-Continued

EO	THL	GRP	THCM	EN	Polarization
3.50	85.0	N0	90.4	6.6	-0.15 ± 0.05
		N1	90.6	6.0	0.04 ± 0.05
		N2	91.1	5.0	-0.15 ± 0.17
		N3	91.4	4.6	-0.04 ± 0.05
		N4	92.5	3.3	-0.05 ± 0.05
	100.0	N0	105.3	6.3	-0.14 ± 0.05
		N1	105.6	5.7	0.01 ± 0.04
		N2	106.1	4.7	0.09 ± 0.21
		N3	106.3	4.4	0.12 ± 0.04
		N4	107.4	3.1	-0.04 ± 0.05
	115.0	N0	119.9	6.0	-0.06 ± 0.05
		N1	120.1	5.4	0.13 ± 0.05
		N2	120.6	4.5	-0.03 ± 0.22
		N3	120.8	4.1	0.31 ± 0.06
		N4	121.8	2.9	-0.10 ± 0.07
	125.0	N0	129.4	5.8	-0.08 ± 0.06
		N1	129.6	5.2	0.05 ± 0.05
		N2	130.1	4.3	0.09 ± 0.40
		N3	130.3	4.0	0.32 ± 0.06
		N4	131.2	2.8	-0.09 ± 0.08
	135.0	N0	138.8	5.7	0.03 ± 0.05
		N1	139.0	5.1	0.00 ± 0.05
		N2	139.4	4.2	0.35 ± 0.20
		N3	139.5	3.9	0.27 ± 0.09
		N4	140.4	2.7	-0.25 ± 0.22

Figure 17. ^{9}Be(d,n) Polarization Angular Distributions

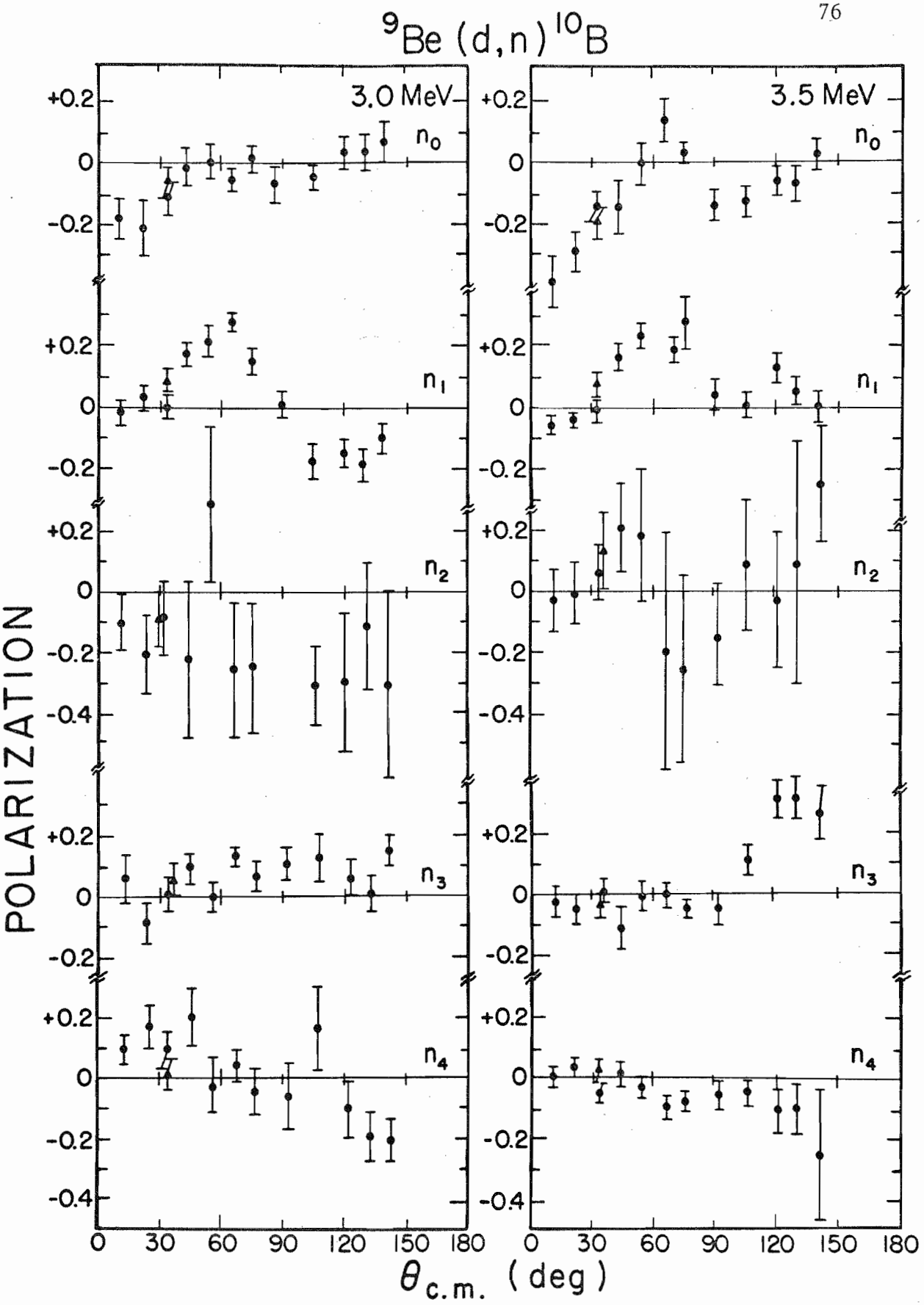
$^{9}Be\,(d,n)\,^{10}B$
3.0 MeV
3.5 MeV
n_0
n_1
n_2
n_3
n_4
POLARIZATION
+0.2
0
-0.2
-0.4
0
30
60
90
120
150
180
$\theta_{c.m.}$ (deg)

determination with the resultant errors in the polarization values. Little information is contained in the polarization values reported for this group, although it does appear from the systematics that P is slightly negative or zero over most of the angular range.

The $^{9}Be(d,n)$ neutron polarization angular distributions exhibit several features of interest. They exhibit a decrease in structure with increasing excitation energy of the residual nucleus at both energies studied. Also, as the bombarding energy increases, the polarization of the n_o group at angles smaller than 50^{o}(c.m.) becomes more negative. No such energy trend can be established for the other neutron groups from the present data. Further, as mentioned in Chapter I, if the $^{9}Be(d,n)^{10}B$ reaction proceeds by the stripping mechanism, the different neutron groups correspond to the transfer of a proton with orbital angular momentum $l_p = 1$ and a total angular momentum of either $j_p = 1/2$ or $3/2$. In particular the n_o and n_2 groups correspond to pure $j_p = 3/2$ transfer while the n_1 and n_3 groups are mixtures of $j_p = 1/2$ and $3/2$ transfers. The n_4 group corresponds to almost pure $j_p = 1/2$ transfer as indicated by the spectroscopic factors in Figure 1. The experimental polarization of the n_1 group at angles smaller than 70^{o}(c.m.) is more positive than the n_o group polarization for the same angles. This fact indicates that the polarization of the $j_p = 1/2$ transfer component of the n_1 polarization is positive at these angles.

The above features form a basic set of characteristics which a computation method such as the DWBA has to predict if it is to be considered a reasonable approximation to reality.

Chapter VI

DWBA CALCULATIONS AND COMPARISON WITH DATA

A. Distorted Wave Born Approximation Method

The theoretical details of DWBA have been treated by many authors including Glendenning (1963), Satchler (1964) and recently by Austern (1970). Only the general outline of the model will be given here.

The basic assumption behind this model is that, in a reaction where only a few internal degrees of freedom of the interacting particles are involved, the predominant process is elastic scattering. Thus, for example, a (d,n) stripping reaction is separated into two parts. In the entrance channel the internal structure of the deuteron is unaltered by the collision with the target nucleus and its center of mass motion can be described by elastic scattering wave functions. In the exit channel, the neutron motion is again described by elastic scattering wave functions. The perturbing potential inducing the transition is taken to be $V_{n,p}$, the nucleon-nucleon potential. The transferred particle is assumed to be captured in a shell-model type potential whose strength is adjusted to duplicate the binding energy of this nucleon in the residual nucleus. Optical model parameters (OMP) obtained from analysis of elastic scattering data for the entrance and exit channels are usually employed in DWBA calculations. This approach, it is felt, gives more physical meaning to

the results than when the OMP are considered as free parameters whose values are determined by the agreement of the DWBA calculations with the data (without requiring that elastic scattering be reproduced by the OMP).

Comparison of DWBA calculations with experiment can yield information about the total angular momentum of the transferred nucleon, the spectroscopic factor, and about which OMP sets correctly describe the elastic scattering wave functions inside the nuclear surface (if the DWBA method is a realistic one for the particular reaction).

B. Neutron Optical Model Parameters

The optical model parameters chosen for the exit channel in the DWBA calculations are based on those of Watson (1969) which represent the results of fitting proton and neutron elastic scattering from 1p shell nuclei for energies from 10 to 50 MeV. They are considered to be sufficiently reliable for the case studied here. As a result these parameters were fixed in all the DWBA calculations. Table 4 lists the set used which was calculated from the energy dependent formulas of Watson (1969). The optical model potential is of the form

$$V(r) = -V_0 f(r, r_0, a_0) + 4 i a_w W_D \frac{d}{dr} f(r, r_w, a_w) + V_{so} \left(\frac{\hbar}{m_\pi c}\right)^2 \frac{1}{r} \frac{d}{dr} f(r, r_{so}, a_{so}) \vec{L} \cdot \vec{\sigma}$$

Values for the parameters chosen here compare favorably with those obtained from other prescriptions such as those of Perey (1963) and Fricke et al. (1967). The functions $f(r, r_i, a_i)$ are the familiar Woods-Saxon potential shapes:

TABLE 4

Optical Model Potential Sets

Set	Particle	V	r	a	W_D	r_w	a_w	V_{so}	r_{so}	a_{so}	r_c
H1	d	108.0	1.15	0.65	6.0	1.20	1.10	12.0	1.15	0.65	1.3
H2	d	140.0	0.85	0.85	14.0	1.66	0.60	12.0	0.85	0.85	1.3
H3	d	150.0	1.20	0.80	16.0	1.80	0.70	8.0	1.20	0.80	1.3
H4	d	80.0	1.58	0.70	14.0	1.85	0.70	8.0	1.58	0.70	1.3
H5	d	85.0	1.30	0.75	14.0	1.55	0.70	8.0	1.30	0.75	1.3
S1	d	110.0	1.00	1.00	6.0	1.90	0.60	8.5	1.00	0.94	1.3
S2	d	118.0	1.00	0.87	7.0	1.50	0.59	5.0	1.00	0.40	1.3
S3	d	105.0	1.10	0.85	8.0	1.60	0.69	8.5	1.00	0.94	1.3
S4	d	120.0	1.02	0.82	8.0	1.50	0.50	5.0	1.00	0.40	1.3
D1	d	102.0	1.15	0.72	10.0	1.72	0.69	10.0	1.80	0.60	1.3
D2	d	130.0	0.85	0.80	7.0	2.10	0.75	6.0	1.20	0.90	1.3
W	n	59.7	1.14	0.57	3.7	1.14	0.50	5.5	1.14	0.57	

$$f(r, r_i, a_i) = \left[1 + \exp\left(\frac{r - r_i A^{\frac{1}{3}}}{a_i}\right)\right]^{-1}$$

where r, r_i and a_i are the radius variable, the nuclear radius parameter (nuclear radius being $R = r_i A^{1/3}$), and the diffuseness.

C. Deuteron Optical Model Potentials

Knowledge about optical model potentials (OMP) for deuteron elastic scattering from light nuclei is meager. One recent study has been reported by Meier et al. (1970) which has significant bearing on the values used below. For ^{9}Be(d,d) there were no OMP sets to choose from for the energy range of the present experiment. In fact, at the time this experiment was undertaken, no ^{9}Be(d,d) elastic scattering data were available below the data at 11.8 MeV of Fitz et al. (1967). In view of this fact ^{9}Be(d,d) data were accumulated at our laboratory by R. A. Hardekopf (unpublished). For energies of 3, 4, 5, and 6 MeV the values are tabulated in Appendix C. The data were analyzed using the Hardekopf and Eastgate (1970) optical model computer code OPTICS. The OM potential form assumed was the same as that for the neutron channel except for the addition of the usual coulomb term with r_c = 1.3 fm. The resulting parameters, sets S1 to S4 in Table 4, all belong to the same Vr_o^n ambiguity potential family. Here n is approximately 1.25. The V_o and r_o of these sets (open circles) are plotted in Figure 18 and compared to the parameter families of Meier (1970) represented by the shaded regions. The OM fits were characteristically poor, especially at the lower energies and at

Figure 18. $^{9}Be(d,d)^{9}Be$ $V_o r_o^n$ Ambiguities

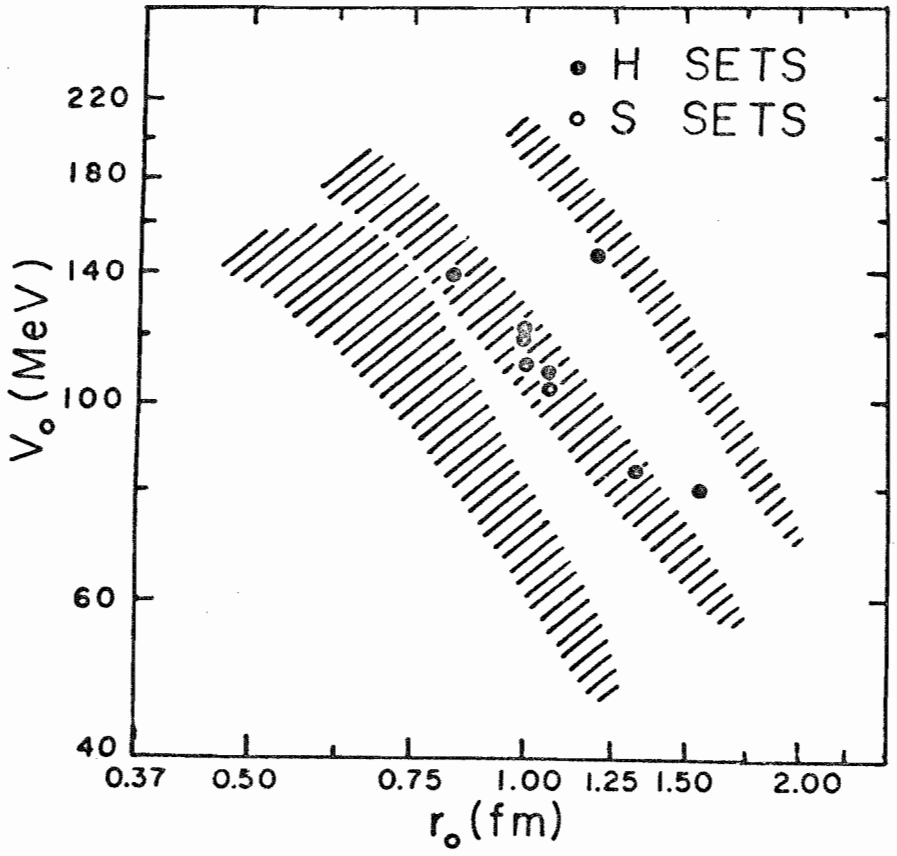
H SETS
S SETS
220
180
140
100
60
40
V_o (MeV)
0.37
0.50
0.75
1.00
1.25
1.50
2.00
r_o (fm)

angles larger than 90^{o} (c.m.). These features are exhibited in Figure 19 where the data and calculated differential cross sections are plotted divided by the coulomb cross section σ_c. The data at angles larger than 90^{o} (c.m.) was especially hard to fit since any attempt to do so resulted in very poor forward angle fits. The calculations at these large angles were especially sensitive to the spin-orbit potential strength V_{so} in contrast with the low sensitivity observed by Meier et al. (1970) in their $^{14}N(d,d)$ calculations. Any attempts to force a fit using OMP sets with different $Vr_{o}^{n}{}_{o}$ values resulted in poorer fits or the variation of the parameters converged to one of the earlier potential sets. The consistent disagreement of the data and calculations at back angles indicated that a compound nucleus contribution was needed in the calculations. This was simulated in the OPTICS program by a Hauser-Feshbach (1952) type contribution with a spin cut-off factor $\sigma^2 = 9$ and a normalization $\frac{D_0}{\Gamma_0}$ varying from 0.4 to 0.8. The data were refitted by T. C. Rhea and R. A. Hardekopf. The σ^2 value was fixed at 9 and the values of $\frac{D_0}{\Gamma_0}$ were varied but no exhaustive attempt was made to optimize this parameter. Sets H1 to H5 in Table 4 resulted from this fitting procedure. The most satisfactory $\frac{D_0}{\Gamma_0}$ value was 0.7. Again these sets (except set H3) belong to the same $Vr_{o}^{n}{}_{o}$ family as shown in Figure 18 (solid circles). Again, any attempt to force fits with different $Vr_{o}^{n}{}_{o}$ values resulted in poorer fits except for set H3. Large V_{so} strengths (8 to 12 MeV) were needed to improve fits at the back angles. However, the data were represented well over the whole range of energies by most of these sets as shown in Figure 20. Here the fits again improved with increasing bombarding energy but the effect is much smaller than with the S

Figure 19. $^{9}Be(d,d)^{9}Be$ Elastic Scattering Optical Model Fits-No H-F Contribution

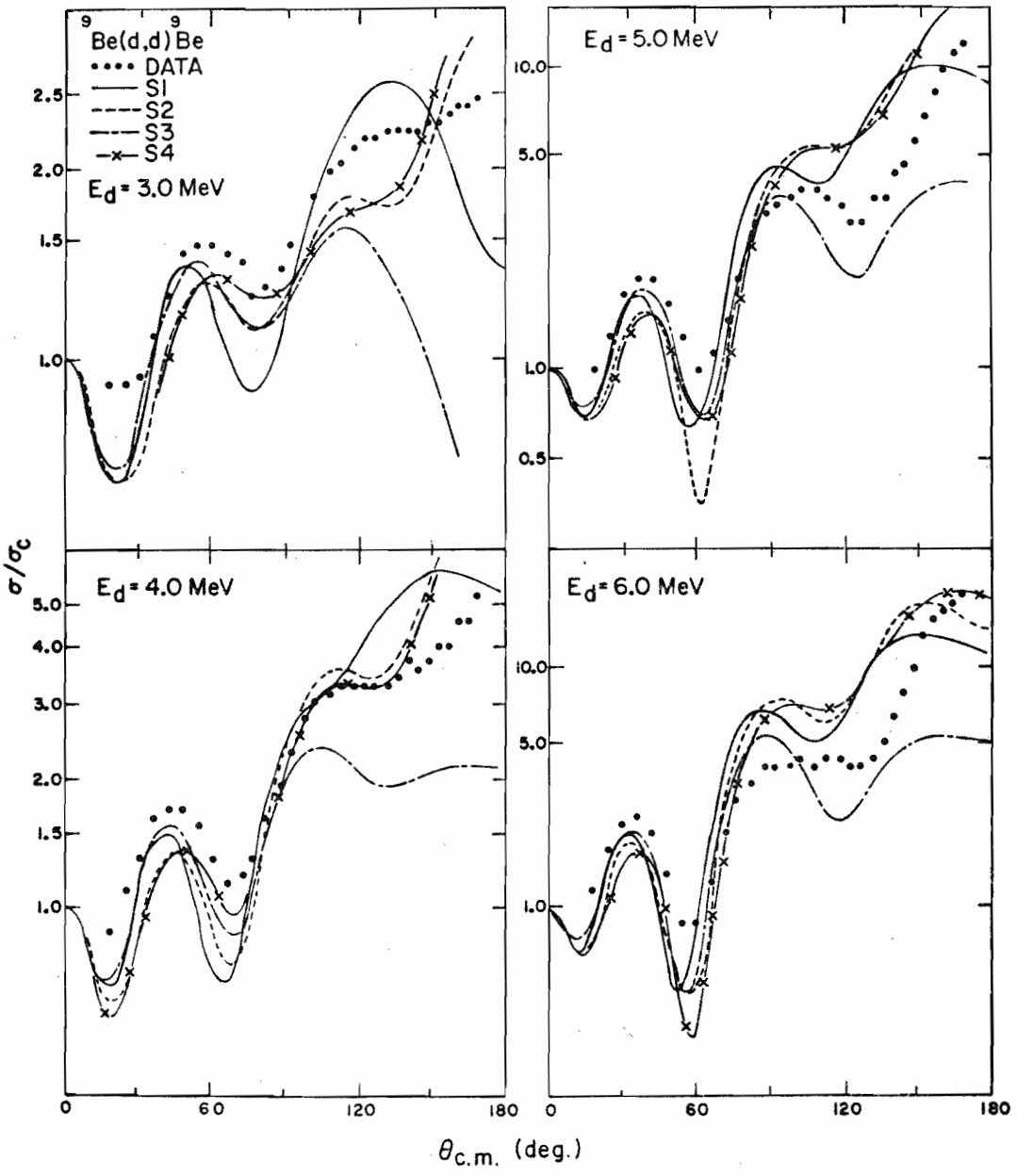
^{9}Be(d,d)^{9}Be
DATA
S1
S2
S3
S4
E_d = 3.0 MeV
E_d = 5.0 MeV
E_d = 4.0 MeV
E_d = 6.0 MeV
σ/σ_c
$\theta_{c.m.}$ (deg.)

Figure 20. $^{9}Be(d,d)^{9}Be$ Elastic Scattering Optical Model Fits- H-F Contribution Included

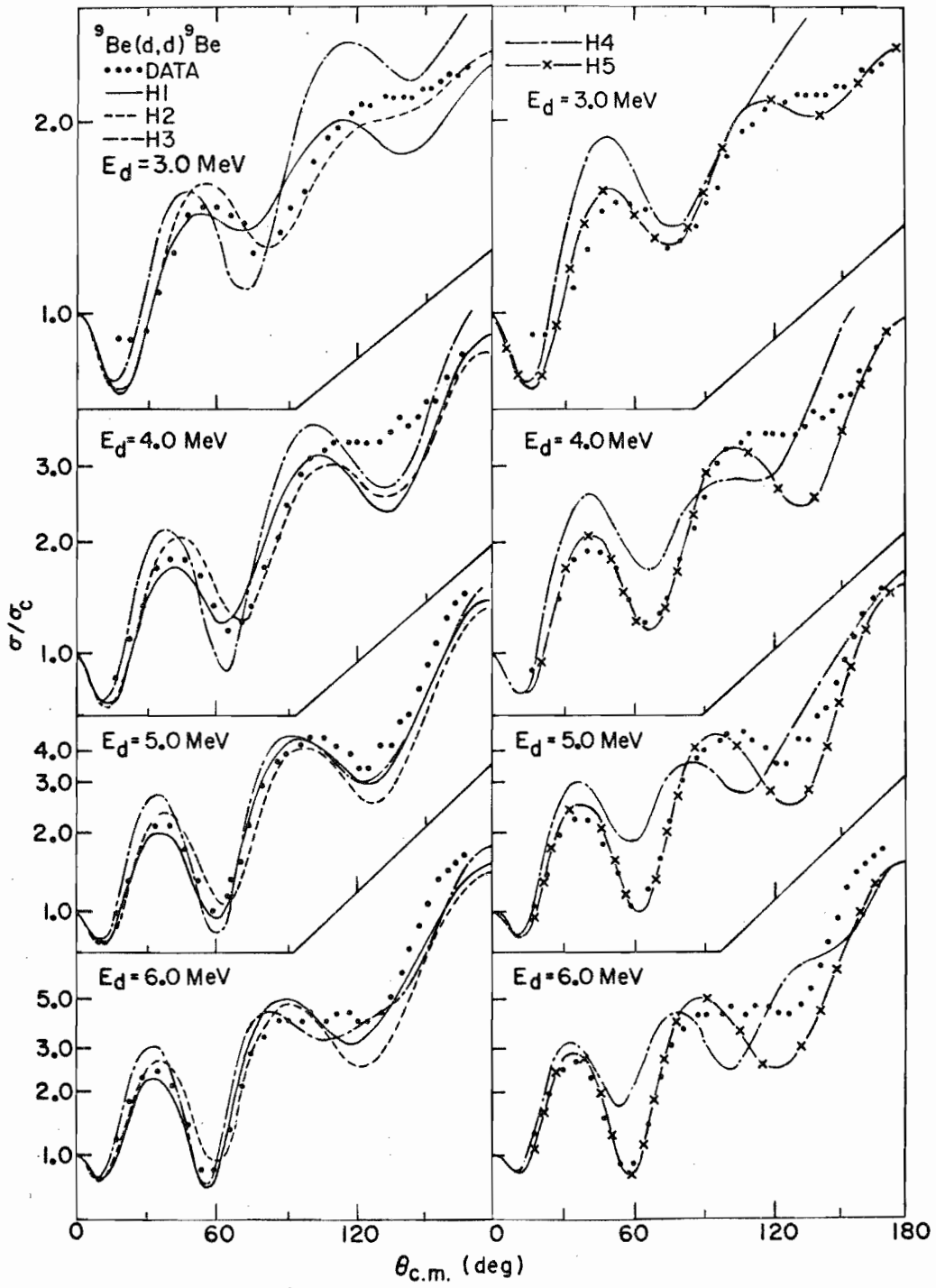
^{9}Be(d,d)^{9}Be
••••DATA
——H1
--- H2
—·—H3
E$_d$ = 3.0 MeV
——H4
—×—H5
E$_d$ = 3.0 MeV
E$_d$ = 4.0 MeV
E$_d$ = 4.0 MeV
E$_d$ = 5.0 MeV
E$_d$ = 5.0 MeV
E$_d$ = 6.0 MeV
E$_d$ = 6.0 MeV
σ/σ$_c$
θ$_{c.m.}$ (deg)
0
60
120
180

set fits (with no H-F contribution). It should be pointed out at this time that no physical significance should be attached to the σ^2 and $\frac{D_0}{\Gamma_0}$ parameters since the applicability of this crude Hauser-Feshbach Theory to a light nucleus such as ^{9}Be is doubtful, especially in view of the many decay channels open to the compound nucleus. The theory was used mainly to simulate the differential cross section shape that would be expected from a compound nucleus contribution to the elastic scattering and the better OM fits vindicated its use. Its inclusion in the calculations did not, surprisingly, introduce OM parameter sets belonging to new $V r_o^n$ families.

The 6 MeV data of Hardekopf (1970) was also compared with OM calculations using parameters from the recent work of Djaloeis et al. (1971). These parameters (D1 and D2, Table 4) were the result of OM fits to their energy-averaged differential cross section and tensor polarization data at 6.3 MeV. However, the OMP sets H1, H2, and H3 yield better over-all fits to both the Hardekopf and the Djaloeis data. Unfortunately, none of the OM sets mentioned fitted the tensor polarization distributions even qualitatively. Even the inclusion of a tensor interaction in the calculations by Djaloeis et al. (1971) produced no resemblance between the calculated tensor polarization and their data. Obviously, much more ^{9}Be(d,d) elastic scattering data (especially polarization data) over a large energy range is needed so that an extensive analysis such as that of Schwandt and Haeberli (1969) on ^{40}Ca(d,d) could be performed. It is felt that only such a study would determine the OM parameters and their energy dependence accurately.

D. DWBA Calculations and Conclusions

The DWBA calculations were made using the code DWUCK of P.D. Kunz. Finite and non-local corrections incorporated in the program were used in all calculations using a finite range parameter of 0.62, a deuteron non-locality parameter of 0.54 and a neutron non-locality parameter of 0.85 as suggested by Kunz. The bound state form factor was calculated using a radius r_o = 1.25 fm, a diffuseness of a_o = 0.63 and a shell model spin-orbit strength of 25.0. The coulomb radius parameter was taken to be r_c = 1.3 fm.

The DWBA calculation results were disappointing. Figure 21 shows comparisons of the DWBA calculations performed at 3.5 MeV with deuteron optical model parameter set H1, the present polarization data, and the cross section data at 4 MeV of Morrison et al. (1961) and that of Siemssen et al. (1965) at 2.82 and 3.14 MeV. The curves have been normalized to each other at the peaks for convenience of comparison. The calculations consistently underestimate the cross section at back angles and display more structure than the data, especially for the higher excited state groups. The polarization results bear no resemblance to the data beyond 60^o (c.m.). Between 60^o and 90^o the DWBA cross section underestimates the experimental cross section, indicating some filling in by compound nucleus contributions. The effect of such filling in would be to dilute the direct reaction polarization if many levels are contributing, or if only a few contribute, the effect can be to cause sizeable polarizations due to interference between the levels themselves and between the compound nucleus and the direct reaction contributions. Thus, we should limit our comparisons of data with the DWBA calculations to angles in the region where the stripping reaction contributes most strongly.

Figure 21. $^{9}Be(d,n)^{10}B$ DWBA Calculations

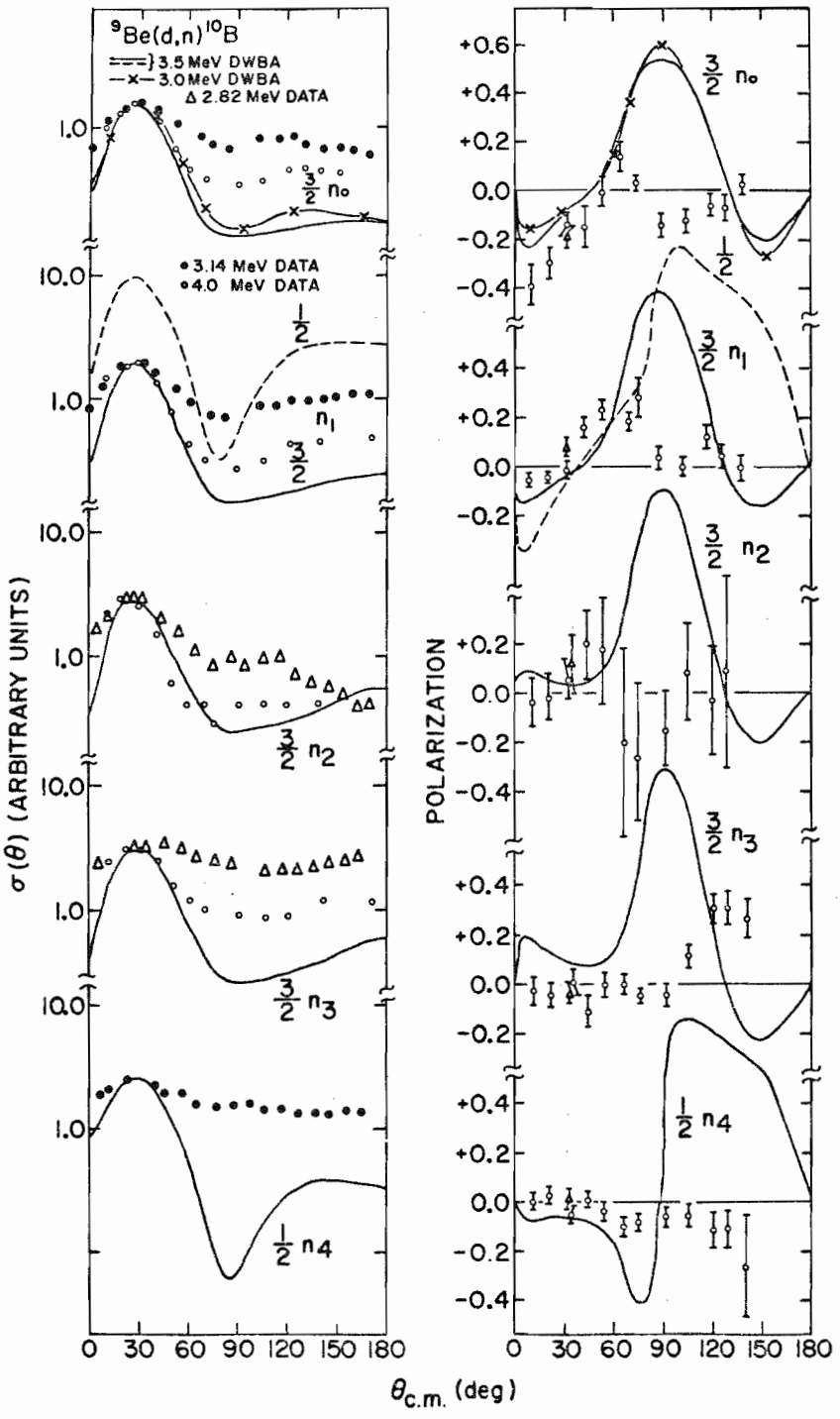
^{9}Be(d,n)^{10}B
3.5 MeV DWBA
3.0 MeV DWBA
Δ 2.62 MeV DATA
• 3.14 MeV DATA
• 4.0 MeV DATA
$\frac{3}{2}$ n0
$\frac{1}{2}$
$\frac{3}{2}$ n1
$\frac{3}{2}$ n2
$\frac{3}{2}$ n3
$\frac{1}{2}$ n4
σ(θ) (ARBITRARY UNITS)
POLARIZATION
θc.m. (deg)

For this forward angle region a Q value dependence is evident with the experimental polarization decreasing in magnitude towards zero as Q decreases. The data have a much larger Q value dependence but the calculations do exhibit the correct energy trend of the cross section and polarization at small angles. Peaking of the calculated cross section at 30^{o} (c.m.) increases with increasing energy and the calculated polarization becomes more negative at forward angles (Figure 21) but again the changes appear to be smaller than corresponding ones in the data. Also, the DWBA j dependence, with the $j_p = 1/2$ transfer component having a more negative value than the $j_p = 3/2$ transfer component contradicts the data. Here, for the n_1 group, the mixture of 1/2 and 3/2 j_p transfers yields a more positive polarization at forward angles than that of the pure $j_p = 3/2$ transfer of the n_o group. The DWBA would predict a more negative value for this polarization. Meier et al. (1970) observed a similar j dependence of the polarization in their $^{14}N(d,n)$ calculations. However, if the Q value of the reaction was increased artificially to 14 MeV in the calculations the j dependence at angles smaller than 60^{o} (c.m.) was reversed, the $j_p = 3/2$ polarization being more negative than the $j_p = 1/2$ polarization. The Q value of the $^{9}Be(d,n)$ reaction is much lower than 14 MeV so such a calculation would be entirely meaningless for this case.

The calculations with the other listed deuteron sets as well as with other neutron sets produced results that had the same characteristic polarization shapes, negative polarization at forward angles for the n_o group and large structure at back angles. Reduction of the deuteron V_{so} reduced the back angle structure somewhat. Yet the O.M. calculations

using these V_{so} values to not reproduce the elastic scattering data. Simultaneous fitting of reaction data with DWBA and elastic scattering data with the optical model is desirable in such a situation but prohibitively costly due to the length of the DWBA calculations. No (d,n) contribution from the compound nucleus was estimated because of the uncertainties in the Hauser-Feshbach parameters and because of the application to a nucleus as light as ^{9}Be (Meier et al., 1970). On the other hand, the inability of the DWBA to predict the general trends of all the data for this and other (d,n) reactions on light nuclei (Taylor 1970, Thomason 1969) suggests that these reactions are perhaps more complex than the DWBA assumes. Certainly the distorted wave approximation becomes less accurate if the bombarding particle is not much lighter than the target. At low energies the perturbation assumed to induce the transition is no longer small compared to the bombarding energy. Furthermore, at the low bombarding energies considered, it is not clear what the compound elastic contribution is to the (d,d) elastic scattering and over what energy range these cross sections should be averaged before extracting valid O.M. analysis. As more data on the ^{9}Be(d,d) and ^{9}Be(d,n) reactions becomes available at higher energies, more tests will be possible to see if 1) the O.M. parameters derived here suitably represent the ^{9}Be(d,d) scattering, and 2) if the DWBA method can be suitably applied to the (d,n) reaction in an (energy) region where the direct reaction becomes more dominant.

APPENDIXES

APPENDIX A

^{9}Be TARGET MAKING PROCEDURES

Pebbles of ^{9}Be were cut into small pieces with a pair of 6" end cutters inside a double polyethylene bag. About 60 mg were placed in a BeO crucible which sat in a tantalum resistance oven in a bell jar. The target backing was made of 0.25 mm thick Ta sheet and was mounted on a water cooled Al block. A movable Ta shield was placed between the target and the crucible during outgassing of the Be and the whole inside of the bell jar was covered with aluminum foil to facilitate clean-up procedures. The distance from the target to the crucible was 10 cm. After outgassing till a vacuum of 10^{-6} torr was obtained the current through the oven was raised until the Be evaporated rapidly (at a pressure less than 5×10^{-6} torr). After all the evaporations had been made, the aluminum foil and all other scrap were sealed in polyethylene bags for disposal. All exposed parts were rinsed briefly in a mild sulfuric acid solution to remove the beryllium metal. This solution and all waste were disposed of by the Duke University Radiation Safety Office. These precautions were taken because beryllium is a carcinogenic material.

The target thicknesses were measured by weighing the target backings before and after evaporation of the beryllium. From the known weight of beryllium deposited the energy loss of 3.0 and 3.5 MeV deuterons in the target was computed.

APPENDIX B

MOTOR-GENERATOR INSTALLATION

The motor-generator installed in the TUNL tandem accelerator laboratory is a ships service set constructed for the U.S. Navy by Westinghouse Electric & Manufacturing Co. It consists of a 115 HP-440 volt three phase 60 cycle A.C. motor and a 75 KW- 120 volt D.C. generator. Manufacturer's part numbers are G.O. WG-43022-L-S.O.4-B-3178. A schematic diagram of the motor-generator set installation is shown on succeeding pages.

Figure 22. Motor-Generator Set Wiring Diagram

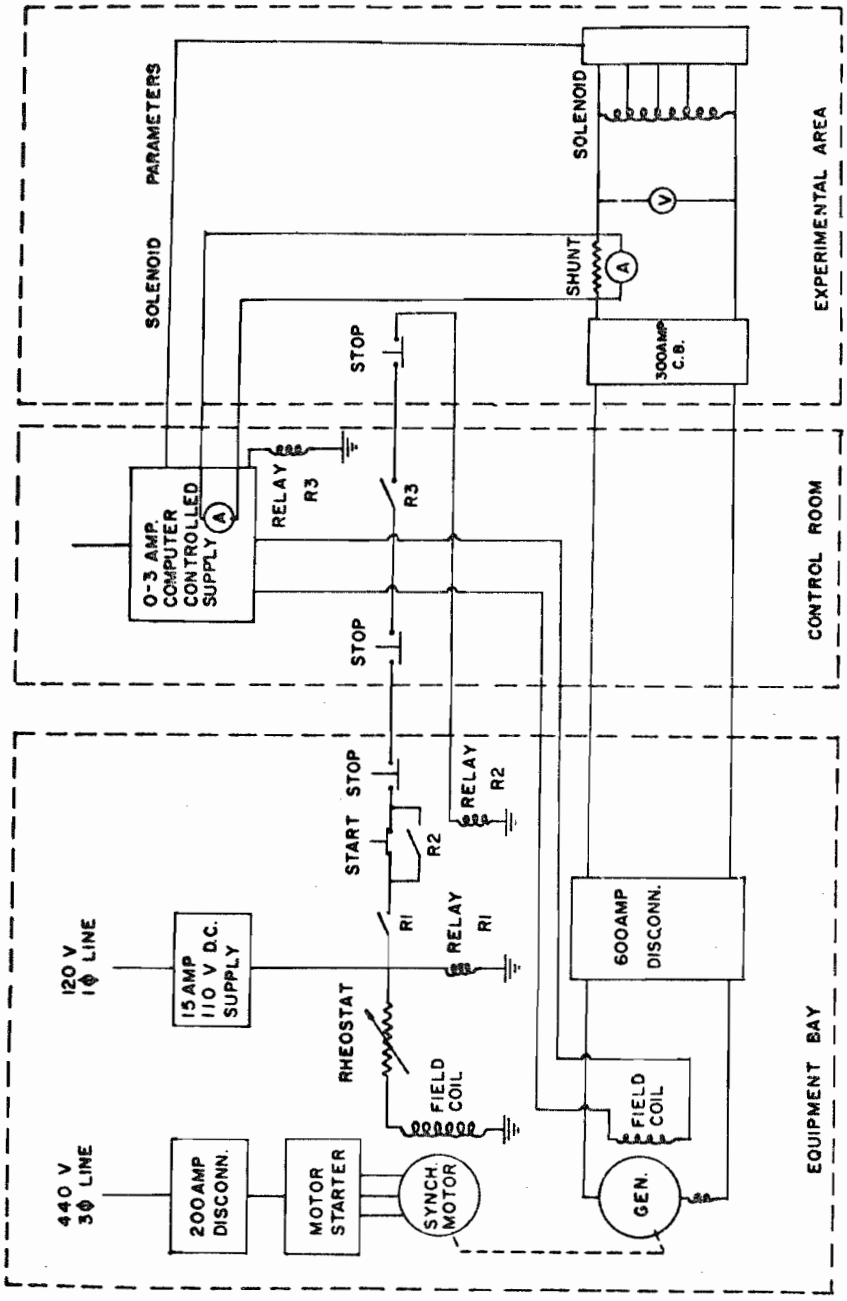
EXPERIMENTAL AREA
CONTROL ROOM
EQUIPMENT BAY
SOLENOID PARAMETERS
SOLENOID
SHUNT
300AMP C.B.
STOP
RELAY R3
R3
0-3 AMP. COMPUTER CONTROLLED SUPPLY
STOP
START STOP
R2
RELAY R2
R1
RELAY R1
120 V 1φ LINE
15 AMP 110 V D.C. SUPPLY
RHEOSTAT
FIELD COIL
600AMP DISCONN.
FIELD COIL
440 V 3φ LINE
200AMP DISCONN.
MOTOR STARTER
SYNCH. MOTOR
GEN.

APPENDIX C

^{9}Be(d,d) ELASTIC CROSS SECTIONS

3.0 to 6.0 MeV deuterons from the TUNL tandem Van de Graaff accelerator were used to bombard a self-supporting beryllium target in a 60 cm scattering chamber. Target thickness, obtained by measuring the energy loss of 5.5 MeV alpha particles was 100 $\mu g/cm^2$. Four cooled silicon surface barrier detectors were used to record data simultaneously at four angles 20° apart. The solid angles were defined by 3.2 x 6.4 mm tantalum collimators, giving an angular resolution of approximately 1.2°.

Data were obtained for deuteron energies of 3.0, 4.0, 5.0 and 6.0 MeV in 5° increments from 15° to 165° to a statistical accuracy better than 1.5%. Northern Scientific analog-to-digital converters and routers interfaced to the TUNL on-line computer were used for data accumulation and analysis. The resolution obtained was sufficient to extract the elastic deuteron peak from competing reactions. A detector fixed at 90° was used to monitor changes in beam current integration and target deterioration. The dead time was recorded for each detector system by using a busy signal from the ADC-router-computer interface. The data were corrected for background under the peaks, monitor counts, and dead time, and were normalized from measured values of target thickness and collimator dimensions. Absolute normalization is ±15%.

TABLE 5

The ^{9}Be(d,d) Elastic Scattering Cross Sections of R. A. Hardekopf, G. Spalek and R. L. Walter

$\theta_{c.m.}$ (deg.)	3.0 MeV σ/σ_c Error	4.0 MeV σ/σ_c Error	5.0 MeV σ/σ_c Error	6.0 MeV σ/σ_c Error
18.32	0.92 ± 0.02	0.89 ± 0.02	0.98 ± 0.02	1.17 ± 0.02
24.39	0.93 ± 0.02	1.08 ± 0.02	1.23 ± 0.02	1.74 ± 0.03
30.43	0.95 ± 0.02	1.29 ± 0.03	1.72 ± 0.03	2.17 ± 0.04
36.43	1.11 ± 0.02	1.62 ± 0.03	1.91 ± 0.04	2.28 ± 0.05
42.38	1.28 ± 0.03	1.72 ± 0.03	1.90 ± 0.04	1.95 ± 0.04
48.27	1.46 ± 0.03	1.73 ± 0.03	1.61 ± 0.03	1.34 ± 0.03
54.11	1.51 ± 0.03	1.54 ± 0.03	1.25 ± 0.03	0.86 ± 0.02
59.87	1.49 ± 0.03	1.32 ± 0.03	0.99 ± 0.02	0.85 ± 0.02
65.56	1.45 ± 0.03	1.15 ± 0.02	1.08 ± 0.02	1.28 ± 0.03
71.18	1.42 ± 0.03	1.19 ± 0.02	1.45 ± 0.03	1.99 ± 0.04
76.76	1.27 ± 0.03	1.33 ± 0.03	1.97 ± 0.04	2.71 ± 0.05
82.14	1.33 ± 0.03	1.59 ± 0.03	2.56 ± 0.05	3.28 ± 0.07
87.48	1.40 ± 0.03	1.94 ± 0.04	3.12 ± 0.06	3.67 ± 0.07
92.73	1.53 ± 0.03	2.34 ± 0.05	3.49 ± 0.07	3.83 ± 0.08
97.88	1.58 ± 0.03	2.68 ± 0.05	3.71 ± 0.07	3.92 ± 0.08
102.93	1.77 ± 0.04	2.93 ± 0.06	3.76 ± 0.08	3.95 ± 0.08
107.88	1.94 ± 0.04	3.13 ± 0.06	3.72 ± 0.07	3.74 ± 0.07
112.73	2.03 ± 0.04	3.24 ± 0.06	3.51 ± 0.07	4.12 ± 0.08
117.48	2.16 ± 0.04	3.20 ± 0.06	3.46 ± 0.07	4.04 ± 0.08
122.14	2.19 ± 0.04	3.28 ± 0.07	2.96 ± 0.06	3.76 ± 0.08
126.70	2.22 ± 0.04	3.29 ± 0.07	3.04 ± 0.06	3.81 ± 0.08
131.17	2.25 ± 0.05	3.22 ± 0.06	3.50 ± 0.07	4.12 ± 0.08
135.56	2.27 ± 0.05	3.45 ± 0.07	3.70 ± 0.07	4.67 ± 0.09
139.87	2.24 ± 0.04	3.67 ± 0.07	4.32 ± 0.09	5.97 ± 0.12
144.10	2.27 ± 0.05	3.52 ± 0.07	4.77 ± 0.10	7.48 ± 0.15
148.27	2.32 ± 0.05	3.74 ± 0.07	5.65 ± 0.11	10.09 ± 0.20
152.37	2.30 ± 0.05	4.00 ± 0.08	6.87 ± 0.14	13.04 ± 0.26
156.42	2.42 ± 0.05	4.06 ± 0.08	8.33 ± 0.17	15.26 ± 0.31
160.43	2.44 ± 0.05	4.52 ± 0.09	9.79 ± 0.20	16.85 ± 0.34
164.39	2.46 ± 0.05	4.57 ± 0.09	10.84 ± 0.22	18.64 ± 0.37
168.32	2.53 ± 0.05	5.15 ± 0.10	12.07 ± 0.24	20.08 ± 0.40

LIST OF REFERENCES

LIST OF REFERENCES

N. V. Alekseev, U. R. Arifkhanov, N. A. Vlasov, V. V. Davydov, and L. N. Samoilov, Soviet Phys. JETP 18 (1964) 979.

N. Austern, Direct Nuclear Reaction Theories, (John Wiley & Sons, Inc., New York, New York, 1969).

N. P. Babenko, I. O. Konstantinov, A. P. Moskalev, and Y. A. Nemilov, Soviet Phys. JETP 20 (1965) 512.

H. H. Barschall, Proceedings of the Second International Symposium on Polarization Phenomena, ed. by P. Huber and H. Schopper (Birkhauser, Basel, 1966), p. 393.

"Basel Convention", Helv. Phys. Act. Supplementum VI, 1961.

J. M. Blatt and L. C. Biedenharn, Rev. Mod. Phys. 24 (1952) 258.

J. E. Brolley, T. M. Putnam and L. Rosen, Phys. Rev. 107 (1957) 820.

S. Cohen and D. Kurath, Nucl. Phys. A101 (1967) 1.

L. Cranberg, A. H. Armstrong, and R. L. Henkel, Phys. Rev. 104 (1956) 1639.

F. S. Dietrich, E. G. Aselberger, and W. E. Meyerhof, Bull. Amer. Phys. Soc. 15 (1970) 495.

A. Djaloeis, J. Cords, and J. Nurzynski, Nucl. Phys. A163 (1971) 131.

P. S. Dubbeldam and R. L. Walter, Nucl. Phys. 28 (1961) 414.

W. Fitz, R. Jahr, and R. Santo, Nucl. Phys. A101 (1967) 449.

J. L. Fowler and J. E. Brolley, Jr., Fast Neutron Physics, ed. by J. L. Fowler and J. B. Marion (Interscience Publishers, New York, 1960), Part I, Chapter I. C.

M. P. Fricke, E. E. Gross, B. J. Morton, and A. Zucker, Phys. Rev. 156 (1967) 1027.

N. K. Glendenning, Ann. Rev. Nucl. Sci. 13 (1963) 191.

H. D. Goldberg and J. M. Le Blanc, Phys. Rev. 119 (1960) 1992.

R. A. Hardekopf, (unpublished Ph.D. dissertation, Duke University, 1971).

R. A. Hardekopf (unpublished).

R. A. Hardekopf and J. Eastgate (unpublished).

W. Hauser and H. Feshbach, Phys. Rev. 87 (1952) 366.

P. Hillman, G. H. Stafford, and C. Whitehead, Nuovo Cimento 4 (1956) 67.

R. G. Kerr and J. D. Anderson, Bull. Amer. Phys. Soc. 13 (1968) 564.

P. D. Kunz (unpublished).

T. H. May, R. L. Walter, and H. H. Barschall, Nucl. Phys. 45 (1963) 17.

M. M. Meier, (unpublished Ph.D. dissertation, Duke University, 1969).

M. M. Meier, R. L. Walter, T. R. Donoghue, R. G. Seyler and R. M. Drisko, Nucl. Phys. A159 (1970) 273.

G. L. Morgan and R. L. Walter, Nucl. Inst. Meth. 58 (1968) 277.

G. C. Morrison, A. T. G. Ferguson, and J. E. Evans, Proceedings of Rutherford International Conference, Manchester, ed. by J. B. Birks (Heywood and Co., 1961), p. 575.

H. Niewodniczanski, J. Szmider, and J. Szymakowski, J. Radium 24 (1963) 871.

F. G. Perey, Phys. Rev. 131 (1963) 745.

F. G. Perey, Proceedings of the Third International Symposium on Polarization Phenomena in Nuclear Reactions, Madison, 1970, ed. by H. H. Barschall and W. Haeberli (Univ. of Wisconsin Press, 1971) p. 131.

L. E. Porter and W. Haeberli, Phys. Rev. 164 (1967) 1229.

F. O. Purser, (unpublished Ph.D. dissertation, Duke University, 1966).

B. V. Rybakov, V. A. Sidorov, and N. A. Vlasov, Nucl Phys. 23 (1961) 491.

G. R. Satchler, Nucl. Phys. 55 (1964) 1.

G. R. Satchler, L. W. Owen, A. J. Elwyn, G. L. Morgan, and R. L. Walter, Nucl Phys. A112 (1968) 1.

P. Schwandt and W. Haeberli, Nucl. Phys. A123 (1969) 401.

R. E. Shamu, Nucl. Instr. Methods 14 (1962) 297.

R. H. Siemssen, M. Cosack, and R. Felst, Nucl. Phys. 69 (1965) 209.

A. Simon and T. Welton, Phys. Rev. 90 (1953) 1036.

Th. Stammbach, R. L. Walter and T. C. Rhea, Proceedings of the Third International Symposium on Polarization Phenomena in Nuclear Reactions, Madison, 1970, ed. by H. H. Barschall and W. Haeberli (Univ. of Wisconsin Press, 1971), p. 556.

J. Taylor, (unpublished Ph.D. dissertation, Duke University, 1971).

R. S. Thomason, (unpublished Ph.D. dissertation, Duke University, 1969).

S. T. Thornton, Nucl. Phys. A136 (1969) 25.

R. L. Walter, Proceedings of the Third International Symposium on Polarization Phenomena in Nuclear Reactions, Madison, 1970, ed. by H. H. Barschall and W. Haeberli, (Univ. of Wisconsin Press, 1971), p. 317.

B. A. Watson and P. P. Singh, Phys. Rev. 182 (1969) 977.

E. P. Wigner, Proceedings of the Third International Symposium on Polarization Phenomena in Nuclear Reactions, Madison, 1970, ed. by H. H. Barschall and W. Haeberli (Univ. of Wisconsin Press, 1971), p. 389.

BIOGRAPHY

George Charles Spalek

Born: October 3, 1940
Prague, Czechoslovakia

Education: B.S. St. Procopius College, 1962
M.S. University of Notre Dame, 1965

Publications:

Polarization of Neutrons Elastically Scattered from ^{3}He at 3.33 and 7.9 MeV (with A. F. Behof and J. M. Hevezi), Nucl. Phys. 84, (1966) 290.

Polarization in n-d Scattering at 7.8 MeV (with J. Taylor, Th.Stammbach, R. Hardekopf, and R. L. Walter), Phys. Rev. 1, (1970) 803.

^{9}Be $(\alpha,n)^{12}$C as a Source of Polarized 7.8 MeV Neutrons (with J. Taylor, Th.Stammbach, and R. L. Walter), Nucl. Inst. & Methods 80, (1970) 304.

Neutron Polarization in the ^{6}Li(d,n) and ^{7}Li(d,n) Reactions for Deuteron Energies from 2.5 to 3.7 MeV (with R. S. Thomason and R. L. Walter) Nucl. Phys. A155 (1970) 659.

Polarization Produced in the ^{9}Be(d,n) Reactions at 3.0 and 3.5 MeV and a Comparison to DWBA Calculations (with R. A. Hardekopf, J. Taylor, Th. Stammbach, and R. L. Walter), Proceedings of the Third International Symposium on Polarization Phenomena in Nuclear Reactions, Madison, 1970, ed. by H. H. Barschall and W. Haeberli (Univ. of Wisconsin Press, 1971), p.749.

Polarization of Neutrons from the D(d,n)^{3}He Reaction from 6 to 14 MeV (with J. Taylor, R. A. Hardekopf, Th. Stammbach, and R. L. Walter), ibid, p.462.

Cross Section and Polarization Measurements for the ^{11}B(d,n_0) and ^{11}B(d,n_1) Reactions from 7 to 12 MeV (with J. Taylor, Th. Stammbach, R. A. Hardekopf, and R. L. Walter), ibid, p.754.

Gas Target Source for Neutron Radiation Therapy (with C. A. Kelsey, M. L. M. Boone, J. M. Hevezi , A. L. Wiley) Radiology, Vol. 98, No. 3, (1971).

The Polarization of Neutrons from the $^{40}Ca(d,n)^{41}Sc(G.S.)$ Reaction at 3.8 MeV (with J. Taylor, Th.Stammbach, and R. L. Walter), (in press).

Neutron Polarization Produced in $^{9}Be(^{3}He,n)$ Reactions for ^{3}He Energies from 2.1 to 3.9 MeV (with R. S. Thomason, L. A. Schaller, and R. L. Walter) (in press).

Measurement of Neutron Polarization from (d,n) Reactions on ^{24}Mg, ^{28}Si, and ^{40}Ca and Comparison to DWBA Calculations (with J. Taylor, Th. Stammbach, and R. L. Walter) (in press).

Four-Nucleon Studies: Part I, A Redetermination of the Neutron Polarization for the $D(d,\pi)^{3}He$ Reaction from 6 to 14 MeV (with R. A. Hardekopf, J. Taylor, Th. Stammbach, and R. L. Walter) (in press).

Scattering of 7.8 MeV Polarized Neutrons from ^{4}He and the Phase Shifts Below 8 MeV (with J. Taylor, Th.Stammbach, R. A. Hardekopf, and R. L. Walter), (to be published).

Abstracts:

Polarization of Neutrons from the $^{9}Be(d,n)^{10}B$ Reaction at 3.0 and 3.5 MeV (with J. Taylor, Th.Stammbach, R. A. Hardekopf and R. L. Walter), Bull. Am. Phys. Soc. 15, (1970) 482.

Neutron Polarization Distributions from the $^{11}B(d,n_0)$ and $^{11}B(d,n_1)$ Reactions at 7.5 and 9.5 MeV (with J. Taylor, Th.Stammbach, R. Hardekopf, and R. L. Walter), Bull. Am. Phys. Soc. 15, (1970) 483.